J. Fluid Mech. (2015), *vol.* 769, *pp.* 590–620.
doi:10.1017/jfm.2015.131

An analytical consideration of steady-state forced convection within a nanofluid-saturated metal foam

W. Zhang[1], W. Li[1] and A. Nakayama[1,2,†]

[1]Department of Mechanical Engineering, Shizuoka University, 3-5-1 Johoku, Naka-ku, Hamamatsu 432-8561, Japan

[2]School of Civil Engineering and Architecture, Wuhan Polytechnic University, Wuhan, Hubei 430023, China

(Received 22 October 2014; revised 9 February 2015; accepted 24 February 2015; first published online 25 March 2015)

An analytical consideration has been made to explore the velocity, temperature and nanoparticle distributions and heat transfer characteristics associated with thermal dispersion and nanoparticle mechanical dispersion within a nanofluid-saturated homogeneous metal foam. A volume-averaging theory was rigorously applied to integrate locally a set of governing equations based on the modified Buongiorno model at the pore scale. Thus, a macroscopic set of volume-averaged governing equations were derived allowing interstitial heat transfer between the nanofluid and metal phases. Unknown terms were modelled mathematically to obtain a closed set of volume-averaged governing equations. Subsequently, a pore-scale analysis was carried out to find possible functional forms for describing thermal dispersion and nanoparticle mechanical dispersion in a nanofluid-saturated metal foam. Using the resulting set of volume-averaged governing equations, forced convective flows in nanofluid-saturated metal foams were analytically investigated for the steady-state case. Eventually, it has been predicted that an unconventionally high level of the heat transfer rate (about 80 times more than the case of base fluid convection without a metal foam) may be achieved by combination of metal foam and nanofluid.

Key words: convection, convection in porous media

1. Introduction

Owing to recent advances in manufacturing technologies, metal foams have become commercially available (Calmidi & Mahajan 1999, 2000; Dukhan 2013). Their main features are high specific surface, high thermal conductivity and comparatively high permeability. Thus, metal foams may well be used as efficient heat exchangers, since they exhibit high interstitial heat transfer between the metal and passing fluid, with a moderate pressure drop.

Nanofluids, on the other hand, have attracted extensive attention for the past decade, in view of their great potential as high-energy carriers resulting from their promising

† Email address for correspondence: tmanaka@ipc.shizuoka.ac.jp

feature of high effective thermal conductivity (e.g. Lee & Choi 1996; Pak & Cho 1998; Lee *et al.* 1999; Xuan & Roetzel 2000; Chien & Chuang 2007; Heris, Esfahany & Etemad 2007; Yang, Li & Nakayama 2013*a*). Hence, it is thought that nanofluid-saturated metal foams, being the combination of metal foams and nanofluids, will lead to a new generation of high-performance heat exchangers.

Sakai, Li & Nakayama (2014) rigorously derived a set of volume-averaged transport equations appropriate for convection in nanofluid-saturated metal foams. However, they assumed local thermal equilibrium between the fluid and metal phases, in which the volume-averaged fluid temperature is assumed to be equal to the metal temperature. In reality, the local thermal equilibrium assumption may fail, since the thermal conductivity of the metal conducting heat from the wall is much higher than that of the nanofluid.

Kuwahara *et al.* (2011) obtained a set of exact solutions for the case of forced convection in a channel filled with a fluid-saturated metal foam, and demonstrated that forced convection in a channel subject to constant wall heat flux must be treated by using a thermal non-equilibrium model, since the fluid and solid phases within the channel are never in thermal equilibrium. This work was followed by that of Yang, Ando & Nakayama (2011), who also compared the set of exact solutions based on local thermal equilibrium against those based on local thermal non-equilibrium models for the case of tube flows, and concluded that substantial errors result from the assumption of local thermal equilibrium for the case of constant heat flux.

Thus, the local thermal equilibrium assumption should be discarded, and a local thermal non-equilibrium model must be introduced with an interstitial heat transfer model between the nanofluid and metal phases.

Another important feature associated with nanofluid-saturated metal foams may be mechanical dispersion (Yang, Liu & Nakayama 2009; Yang & Nakayama 2010). Mechanical dispersion in heat transfer resulting from porous matrices is termed ‘thermal dispersion’, whereas, in this study, mechanical dispersion in nanoparticle transport may be called ‘nanoparticle mechanical dispersion’, i.e. macroscopic dispersion resulting from porous matrices. (This should not be confused with ‘nanoparticle dispersion’, meaning particles dispersed in the base fluid, i.e. microscopic dispersion.)

In this study, we shall derive an appropriate set of volume-averaged transport equations for convection in nanofluid-saturated metal foams, using a volume-averaging theory and allowing the nanofluid temperature and the metal temperature to differ from each other, i.e. local thermal non-equilibrium model. The microscopic transport equations based on the Buongiorno model (Buongiorno 2006) for convective heat transfer in nanofluids are modified so as to fully account for the effects of nanoparticle volume fraction distributions on the continuity, momentum and energy equations, and then are integrated within a local averaging volume to obtain an appropriate set of governing equations in terms of volume-averaged dependent variables (Cheng 1978; Quintard & Whitaker 1993; Nakayama 1995; Quintard & Whitaker 1995). Non-zero terms associated with interfacial surface integrals (Nakayama, Kuwahara & Hayashi 2004) and averages of spatial deviations are subsequently modelled mathematically using the volume-averaged dependent variables.

A pore-scale analysis will be conducted to deduce possible functional forms for describing thermal dispersion in a nanofluid-saturated metal foam. Moreover, nanoparticle mechanical dispersion (i.e. macroscopic dispersion resulting from porous matrices) will be focused upon for the first time, and will be modelled mathematically, considering a pore-scale conduit. It will be analytically shown that the longitudinal

particle mechanical dispersion works either to suppress or to enhance effective diffusion depending on the sign of the local phase temperature difference, while the transverse counterpart is insignificant and therefore can be neglected. Furthermore, heat transfer performance evaluation under equal pumping power will be made for the case of forced convective heat transfer in a nanofluid-saturated metal foam. We shall demonstrate that an unconventionally high level of the heat transfer rate (about 80 times more than the case of base fluid convection without a metal foam) is attainable by combining a metal foam with a nanofluid.

2. Modified Buongiorno equations for nanofluids

Buongiorno (2006) assumed incompressible flow, no chemical reactions, negligible external forces, dilute mixture, negligible viscous dissipation, negligible radiative heat transfer, and local thermal equilibrium between nanoparticles and base fluid. Local thermal equilibrium between the nanoparticles and the base fluid is obvious since the size of the nanoparticles is so small that nanoparticle temperature changes instantly and coincides with that of the surrounding base fluid. Following Yang *et al.* (2013*b*), the two-component mixture model proposed by Buongiorno may be modified to allow nanofluid density variation in mass, momentum and energy conservations as

$$\frac{\partial \rho u_j}{\partial x_j} = 0, \tag{2.1}$$

$$\frac{\partial \rho u_i}{\partial t} + \frac{\partial \rho u_j u_i}{\partial x_j} = -\frac{\partial p}{\partial x_i} + \frac{\partial}{\partial x_j}\mu\left(\frac{\partial u_i}{\partial x_j} + \frac{\partial u_j}{\partial x_i}\right), \tag{2.2}$$

$$c\left(\frac{\partial \rho T}{\partial t} + \frac{\partial \rho u_j T}{\partial x_j}\right) = \frac{\partial}{\partial x_j}\left(k\frac{\partial T}{\partial x_j}\right), \tag{2.3}$$

$$\rho_p\left(\frac{\partial \phi}{\partial t} + \frac{\partial u_j \phi}{\partial x_j}\right) = \frac{\partial}{\partial x_j}\left(\rho_p D_B \frac{\partial \phi}{\partial x_j} + \frac{\rho_p D_T}{T}\frac{\partial T}{\partial x_j}\right), \tag{2.4}$$

where ρ, c, μ and k are the density, heat capacity, viscosity and thermal conductivity of the nanofluid, which depend on the nanoparticle volume fraction ϕ as

$$\rho = \phi\rho_p + (1-\phi)\rho_{bf}, \tag{2.5a}$$

$$c = [\phi\rho_p c_p + (1-\phi)\rho_{bf} c_{bf}]/\rho, \tag{2.5b}$$

$$\mu = \mu_{bf}(1 + a_\mu\phi + b_\mu\phi^2) = \mu_{bf}(1 + 7.3\phi + 123\phi^2), \tag{2.5c}$$

$$k = k_{bf}(1 + a_k\phi + b_k\phi^2) = k_{bf}(1 + 2.72\phi + 4.97\phi^2). \tag{2.5d}$$

The Brownian and thermophoretic diffusion coefficients are given by

$$D_B = \frac{k_{BO}T}{3\pi\mu_{bf}d_p} \tag{2.6a}$$

and

$$D_T = 0.26\frac{k_{bf}}{2k_{bf} + k_p}\frac{\mu_{bf}}{\rho_{bf}}\phi, \tag{2.6b}$$

respectively. The nanofluid thermophysical properties such as μ and k are considered as given functions of ϕ. Equations (2.5*c*) and (2.5*d*) are what appear to be the most reliable correlations proposed by Maiga *et al.* (2005), where the subscripts p and bf refer to nanoparticle and base fluid, respectively. Moreover, k_{BO} is the Boltzmann constant and d_p is the nanoparticle diameter, which can be anywhere of the order

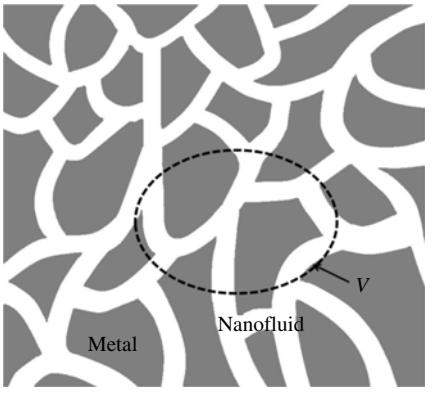

FIGURE 1. The averaging volume in a nanofluid-saturated metal foam. The averaging volume is smaller than the macroscopic characteristic scale but larger than the pore scale.

of 1–100 nm. As for the temperature dependence of thermophysical properties, Li & Nakayama (2015) investigated the effect of temperature-dependent thermophysical properties on convective heat transfer rates. They found that variations of base fluid properties due to temperature variation are small enough to be neglected compared with the effects of nanoparticle volume fraction and temperature.

Many, including Bianco *et al.* (2009), have found that the two-component mixture model is quite adequate for describing nanofluid heat transfer, as supported by Buongiorno (2006) using a magnitudes analysis. The energy equation (2.3) appears to be identical to that of a pure fluid, except that all properties are functions of ϕ. It should be noted that the nanoparticle continuity equation (2.4) must be treated simultaneously with (2.1)–(2.3) for the other dependent variables, since the thermophysical properties strongly depend on the spatial distribution of ϕ. Most previous researchers neglected the spatial variations of thermophysical properties, including Brownian and thermophoretic diffusion coefficients. Such analytical treatments could result in substantial errors, as discussed in Yang *et al.* (2013*b*). In this study, all these variations will be considered.

3. Volume-averaging theory

A volume-averaging procedure may be used to derive a complete set of macroscopic governing equations for convection within a nanofluid-saturated metal foam. Let us consider a local averaging volume V in a nanofluid-saturated metal foam, as shown in figure 1, whose length scale $V^{1/3}$ is much smaller than the macroscopic characteristic length, but, at the same time, much greater than the microscopic characteristic length (see e.g. Cheng 1978; Quintard & Whitaker 1993, 1995; Nakayama 1995). Under this condition, the volume average of a certain variable φ is defined as

$$\langle\varphi\rangle = \frac{1}{V}\int_{V_f}\varphi \mathrm{d}V. \tag{3.1a}$$

Another average, namely, the intrinsic average, is given by

$$\langle\varphi\rangle^f = \frac{1}{V_f}\int_{V_f}\varphi \mathrm{d}V \tag{3.1b}$$

where V_f is a volume space that the nanofluid occupies. Obviously, the two averages are related as $\langle\varphi\rangle = \varepsilon\langle\varphi\rangle^f$, where $\varepsilon = V_f/V$ is the porosity, namely, the local volume fraction of the nanofluid phase. We decompose a variable into its intrinsic average and the spatial deviation from it:

$$\varphi = \langle\varphi\rangle^f + \tilde{\varphi}. \tag{3.2}$$

All dependent variables in the microscopic governing equations for the nanofluid and metal phases will be decomposed in this manner. We shall utilize the following spatial average relationships:

$$\langle\varphi_1\varphi_2\rangle^f = \langle\varphi_1\rangle^f\langle\varphi_2\rangle^f + \langle\tilde{\varphi}_1\tilde{\varphi}_2\rangle^f \tag{3.3}$$

$$\left\langle\frac{\partial\varphi}{\partial x_i}\right\rangle = \frac{\partial\langle\varphi\rangle}{\partial x_i} + \frac{1}{V}\int_{A_{int}}\varphi n_i \mathrm{d}A \quad \text{or} \quad \left\langle\frac{\partial\varphi}{\partial x_i}\right\rangle^f = \frac{1}{\varepsilon}\frac{\partial\varepsilon\langle\varphi\rangle^f}{\partial x_i} + \frac{1}{V_f}\int_{A_{int}}\varphi n_i \mathrm{d}A \tag{3.4a,b}$$

and

$$\left\langle\frac{\partial\varphi}{\partial t}\right\rangle = \frac{\partial\langle\varphi\rangle}{\partial t}. \tag{3.5}$$

Here A_{int} represents the interfaces between fluid and solid matrix within a local averaging volume. Note that n_i is the unit vector pointing outwards from the nanofluid side to the solid side. All dependent variables for nanofluid and metal phases are decomposed according to (3.2). Then, the microscopic equations (2.1)–(2.4) are integrated over a local averaging volume, exploiting the foregoing spatial average relationships. The set of macroscopic governing equations thus obtained for nanofluid and metal phases in a nanofluid-saturated metal foam with uniform porosity ε may be given as follows:

$$\frac{\partial\rho\langle u_j\rangle^f}{\partial x_j} + \frac{1}{V_f}\int_{A_{int}}\rho u_j n_j \mathrm{d}A = 0, \tag{3.6}$$

$$\begin{aligned}
&\frac{\partial\rho\langle u_i\rangle^f}{\partial t} + \frac{\partial\rho\langle u_j\rangle^f\langle u_i\rangle^f}{\partial x_j} \\
&\quad = -\frac{\partial\langle p\rangle^f}{\partial x_i} + \frac{\partial}{\partial x_j}\left(\mu\left(\frac{\partial\langle u_i\rangle^f}{\partial x_j} + \frac{\partial\langle u_j\rangle^f}{\partial x_i}\right) + \frac{\mu}{V_f}\int_{A_{int}}(u_i n_j + u_j n_i)\mathrm{d}A - \rho\langle\tilde{u}_i\tilde{u}_j\rangle^f\right) \\
&\qquad + \frac{1}{V_f}\int_{A_{int}}\left(\mu\left(\frac{\partial u_i}{\partial x_j} + \frac{\partial u_j}{\partial x_i}\right) - p\delta_{ij}\right)n_j \mathrm{d}A - \frac{1}{V_f}\int_{A_{int}}\rho u_j u_i n_j \mathrm{d}A,
\end{aligned} \tag{3.7}$$

$$\begin{aligned}
&\varepsilon c\left(\frac{\partial\rho\langle T\rangle^f}{\partial t} + \frac{\partial\rho\langle u_j\rangle^f\langle T\rangle^f}{\partial x_j}\right) \\
&\quad = \frac{\partial}{\partial x_j}\left(\varepsilon k\frac{\partial\langle T\rangle^f}{\partial x_j} + \frac{k}{V}\int_{A_{int}} T n_j \mathrm{d}A - \varepsilon\rho c\langle\tilde{T}\tilde{u}_j\rangle^f\right) \\
&\qquad + \frac{1}{V}\int_{A_{int}} k\frac{\partial T}{\partial x_j}n_j \mathrm{d}A - \frac{c}{V}\int_{A_{int}}\rho T u_j n_j \mathrm{d}A,
\end{aligned} \tag{3.8}$$

$$(1-\varepsilon)c_s\frac{\partial\langle T\rangle^s}{\partial t} = \frac{\partial}{\partial x_j}\left((1-\varepsilon)k_s\frac{\partial\langle T\rangle^s}{\partial x_j} - \frac{k_s}{V}\int_{A_{int}} T n_j \mathrm{d}A\right) - \frac{1}{V}\int_{A_{int}} k_s\frac{\partial T}{\partial x_j}n_j \mathrm{d}A \tag{3.9}$$

$$\frac{\partial \langle \phi \rangle^f}{\partial t} + \frac{\partial \langle u_j \rangle^f \langle \phi \rangle^f}{\partial x_j}$$
$$= \frac{\partial}{\partial x_j}\left(D_B \frac{\partial \langle \phi \rangle^f}{\partial x_j} + \frac{D_T}{\langle T \rangle^f}\frac{\partial \langle T \rangle^f}{\partial x_j} + \frac{D_B}{V_f}\int_{A_{int}} \phi n_j \mathrm{d}A + \frac{D_T}{V_f \langle T \rangle^f}\int_{A_{int}} T n_j \mathrm{d}A - \langle \tilde{\phi}\tilde{u}_j \rangle^f \right)$$
$$+ \frac{1}{V_f}\int_{A_{int}} \left(D_B \frac{\partial \phi}{\partial x_j} + \frac{D_T}{\langle T \rangle^f}\frac{\partial T}{\partial x_j} \right) n_j \mathrm{d}A - \frac{1}{V_f}\int_{A_{int}} u_j \phi n_j \mathrm{d}A. \tag{3.10}$$

Equation (3.9) is obtained by integrating the conduction equation in a metal phase. In the foregoing equations, many interfacial terms vanish due to no-slip and no-particle flux conditions on the nanofluid–metal interface, namely,

$$u_j = \mathbf{0} \quad \text{and} \quad \left(D_B \frac{\partial \phi}{\partial x_j} + \frac{D_T}{T}\frac{\partial T}{\partial x_j} \right) n_j = 0. \tag{3.11a,b}$$

Thus, many surface integral terms vanish and the equations reduce to

$$\frac{\partial \rho \langle u_j \rangle^f}{\partial x_j} = 0, \tag{3.12}$$

$$\frac{\partial \rho \langle u_i \rangle^f}{\partial t} + \frac{\partial \rho \langle u_j \rangle^f \langle u_i \rangle^f}{\partial x_j}$$
$$= -\frac{\partial \langle p \rangle^f}{\partial x_i} + \frac{\partial}{\partial x_j}\left(\mu \left(\frac{\partial \langle u_i \rangle^f}{\partial x_j} + \frac{\partial \langle u_j \rangle^f}{\partial x_i} \right) - \rho \langle \tilde{u}_i \tilde{u}_j \rangle^f \right)$$
$$+ \frac{1}{V_f}\int_{A_{b_{int}}} \left(\mu \left(\frac{\partial u_i}{\partial x_j} + \frac{\partial u_j}{\partial x_i} \right) - p\delta_{ij} \right) n_j \mathrm{d}A, \tag{3.13}$$

$$\varepsilon c \left(\frac{\partial \rho \langle T \rangle^f}{\partial t} + \frac{\partial \rho \langle u_j \rangle^f \langle T \rangle^f}{\partial x_j} \right)$$
$$= \frac{\partial}{\partial x_j}\left(\varepsilon k \frac{\partial \langle T \rangle^f}{\partial x_j} + \frac{k}{V}\int_{A_{int}} T n_j \mathrm{d}A - \varepsilon \rho c \langle \tilde{T}\tilde{u}_j \rangle^f \right) + \frac{1}{V}\int_{A_{int}} k \frac{\partial T}{\partial x_j} n_j \mathrm{d}A, \tag{3.14}$$

$$(1-\varepsilon) c_s \frac{\partial \rho \langle T \rangle^s}{\partial t} = \frac{\partial}{\partial x_j}\left((1-\varepsilon) k_s \frac{\partial \langle T \rangle^s}{\partial x_j} - \frac{k_s}{V}\int_{A_{int}} T n_j \mathrm{d}A \right) - \frac{1}{V}\int_{A_{int}} k \frac{\partial T}{\partial x_j} n_j \mathrm{d}A, \tag{3.15}$$

$$\varepsilon \left(\frac{\partial \langle \phi \rangle^f}{\partial t} + \frac{\partial \langle u_j \rangle^f \langle \phi \rangle^f}{\partial x_j} \right)$$
$$= \frac{\partial}{\partial x_j}\left(\varepsilon D_B \frac{\partial \langle \phi \rangle^f}{\partial x_j} + \frac{\varepsilon D_T}{\langle T \rangle^f}\frac{\partial \langle T \rangle^f}{\partial x_j} + \frac{D_B}{V}\int_{A_{int}} \phi n_j \mathrm{d}A + \frac{D_T}{V \langle T \rangle^f}\int_{A_{int}} T n_j \mathrm{d}A - \varepsilon \langle \tilde{\phi}\tilde{u}_j \rangle^f \right). \tag{3.16}$$

In the previous equations, the correlations associated with deviations, $-\rho \langle \tilde{u}_i \tilde{u}_j \rangle^f$, $-\varepsilon \rho c \langle \tilde{T}\tilde{u}_j \rangle^f$ and $-\varepsilon \langle \tilde{\phi}\tilde{u}_j \rangle^f$, correspond to mechanical dispersion terms, whereas the surface integral terms, $(k/V)\int_{A_{int}} T n_j \mathrm{d}A$, $(D_B/V)\int_{A_{int}} \phi n_j \mathrm{d}A$ and $(D_T/(V\langle T \rangle^f))\int_{A_{int}} T n_j \mathrm{d}A$, correspond to the tortuosity terms.

4. Mathematical modelling

As usual, the Forchheimer-extended Darcy law is introduced to describe the internal flow resistance:

$$\frac{1}{V_f}\int_{A_{int}}\left(\mu\left(\frac{\partial u_i}{\partial x_j}+\frac{\partial u_j}{\partial x_i}\right)-p\delta_{ij}\right)n_j\mathrm{d}A\,\frac{\partial}{\partial x}\rho\langle\tilde{u}_i\tilde{u}_j\rangle^f=-\frac{\varepsilon\mu}{K}\langle u_j\rangle^f-\rho\varepsilon^2 b\sqrt{\langle u_k\rangle^f\langle u_k\rangle^f}\langle u_j\rangle^f, \tag{4.1}$$

while tortuosity in nanoparticle volume fraction transport is neglected since

$$\frac{D_B}{V_f}\int_{A_{int}}\phi n_j\mathrm{d}A\cong\frac{D_B}{V_f}\phi\int_{A_{int}}n_j\mathrm{d}A=\mathbf{0}. \tag{4.2}$$

The tortuosity terms in the two energy equations may be modelled by introducing the Yang–Nakayama effective porosity ε^* (Yang & Nakayama 2010; Kuwahara *et al.* 2011) as

$$\varepsilon k\frac{\partial\langle T\rangle^f}{\partial x_j}+\frac{k}{V}\int_{A_{int}}Tn_j\mathrm{d}A=\varepsilon^* k\frac{\partial\langle T\rangle^f}{\partial x_j}, \tag{4.3a}$$

$$(1-\varepsilon)k_s\frac{\partial\langle T\rangle^s}{\partial x_j}-\frac{k_s}{V}\int_{A_{int}}Tn_j\mathrm{d}A=(1-\varepsilon^*)k_s\frac{\partial\langle T\rangle^s}{\partial x_j}, \tag{4.3b}$$

and the effective porosity may easily be evaluated from

$$\varepsilon^*=\frac{k_s-k_{stag}}{k_s-k_f} \tag{4.4}$$

where k_{stag} is the stagnant thermal conductivity of the saturated porous medium, which can readily be measured using a standard method. However, for the cases of high-conductivity porous media, such as metal foams, satisfying the condition $k_s/k\gg 3/(1-\varepsilon)$, there is no need to measure the stagnant thermal conductivity of the saturated porous medium, since the effective porosity may be approximated well by

$$\varepsilon^*=\frac{2+\varepsilon}{3} \tag{4.5}$$

according to Yang & Nakayama (2010). For example, in the case of the combination of aluminium foam and water, we typically have $k_s/k\cong 330$ and $\varepsilon=0.90$. Thus, $k_s/k\gg 3/(1-\varepsilon)$ is satisfied such that $\varepsilon^*=(2+0.9)/3=0.97$. Furthermore, Newton's cooling law may be adopted for the interstitial heat transfer between the nanofluid phase and the metal foam as

$$\frac{1}{V}\int_{A_{int}}k\frac{\partial T}{\partial x_j}n_j\mathrm{d}A=h_v(\langle T\rangle^s-\langle T\rangle^f), \tag{4.6}$$

where h_v is the volumetric interstitial heat transfer coefficient. Upon implementing the foregoing mathematical models, the equations reduce to

$$\frac{\partial\rho\langle u_j\rangle}{\partial x_j}=0, \tag{4.7}$$

$$\frac{1}{\varepsilon}\frac{\partial \rho\langle u_i\rangle}{\partial t}+\frac{1}{\varepsilon^2}\frac{\partial \rho\langle u_j\rangle\langle u_i\rangle}{\partial x_j}=-\frac{\partial\langle p\rangle^f}{\partial x_i}+\frac{\partial}{\partial x_j}\left(\frac{\mu}{\varepsilon}\frac{\partial\langle u_i\rangle}{\partial x_j}\right)-\frac{\mu}{K}\langle u_i\rangle-\rho b\sqrt{\langle u_k\rangle\langle u_k\rangle}\langle u_i\rangle, \tag{4.8}$$

$$\varepsilon c\frac{\partial \rho\langle T\rangle^f}{\partial t}+c\frac{\partial \rho\langle u_j\rangle\langle T\rangle^f}{\partial x_j}=\frac{\partial}{\partial x_j}\left(\varepsilon^* k_f\frac{\partial\langle T\rangle^f}{\partial x_j}-\varepsilon\rho c\langle\tilde{T}\tilde{u}_j\rangle^f\right)-h_v(\langle T\rangle^f-\langle T\rangle^s), \tag{4.9}$$

$$(1-\varepsilon)\rho_s c_s\frac{\partial\langle T\rangle^s}{\partial t}=\frac{\partial}{\partial x_j}(1-\varepsilon^*)k_s\frac{\partial\langle T\rangle^s}{\partial x_j}-h_v(\langle T\rangle^s-\langle T\rangle^f)=0, \tag{4.10}$$

$$\varepsilon\frac{\partial\langle\phi\rangle^f}{\partial t}+\frac{\partial\langle u_j\rangle\langle\phi\rangle^f}{\partial x_j}=\frac{\partial}{\partial x_j}\left(\varepsilon D_B\frac{\partial\langle\phi\rangle^f}{\partial x_j}+\frac{\varepsilon^* D_T}{\langle T\rangle^f}\frac{\partial\langle T\rangle^f}{\partial x_j}-\varepsilon\langle\tilde{\phi}\tilde{u}_j\rangle^f\right). \tag{4.11}$$

Note that (4.3*a*) is exploited to express the particle tortuosity term as

$$\begin{aligned}\frac{\varepsilon D_T}{\langle T\rangle^f}\frac{\partial\langle T\rangle^f}{\partial x_j}+\frac{D_T}{V\langle T\rangle^f}\int_{A_{int}}Tn_j\mathrm{d}A &\cong \frac{\varepsilon D_T}{\langle T\rangle^f}\frac{\partial\langle T\rangle^f}{\partial x_j}+(\varepsilon^*-\varepsilon)\frac{D_T}{\langle T\rangle^f}\frac{\partial\langle T\rangle^f}{\partial x_j}\\ &= \frac{\varepsilon^* D_T}{\langle T\rangle^f}\frac{\partial\langle T\rangle^f}{\partial x_j}.\end{aligned} \tag{4.12}$$

In the foregoing equations, the Darcian velocity vector $\langle u_j\rangle=\varepsilon\langle u_j\rangle^f$ is used in place of the intrinsic velocity vector $\langle u_j\rangle^f$.

5. Thermal dispersion

Our remaining task in mathematical modelling is to express the mechanical dispersion terms, namely, $-\varepsilon\rho c\langle\tilde{T}\tilde{u}_j\rangle^f$ and $-\varepsilon\langle\tilde{\phi}\tilde{u}_j\rangle^f$, in terms of determinable variables. However, measurement of mechanical dispersion is quite formidable. A limited number of correlations for metal foams are available, and only for transverse thermal dispersion. No empirical information is available for longitudinal thermal dispersion in metal foams. As for the nanoparticle mechanical dispersion, neither theoretical nor empirical information has been reported so far. Yang & Nakayama (2010) pointed out that the volumetric interstitial heat transfer coefficient is comparatively easy to measure, using a standard method such as the single blow method (Liang & Yang 1975). Thus, they carried out an analytical consideration at pore scale, and derived a theoretical relation to estimate thermal dispersion from the volumetric interstitial heat transfer coefficient, as illustrated below.

Along the macroscopic flow direction x, the nanofluid phase energy equation (4.9) at steady state may be written as

$$c\rho\langle u\rangle\frac{\partial\langle T\rangle^f}{\partial x}\cong -h_v(\langle T\rangle^f-\langle T\rangle^s). \tag{5.1}$$

We have dropped the diffusion term, since the convection term on the left-hand side predominates over the axial diffusion term. A magnitude analysis (Yang & Nakayama 2010) reveals that the diffusive term in (4.9) may be neglected as a first approximation, when the external scale of the flow system is much larger than the pore scale. We shall consider a pore-scale passage as illustrated in figure 2. The longitudinal thermal dispersion term may be evaluated using the microscopic velocity and temperature profiles prevailing in this pore-scale passage as follows:

$$\begin{aligned}-\varepsilon\rho c\langle\tilde{T}\tilde{u}\rangle^f &= -\rho c\langle u\rangle(\langle T\rangle^f-\langle T\rangle^s)\langle(f-1)(g-1)\rangle^f\\ &= \frac{(\rho c\langle u\rangle)^2}{h_v}\langle(f-1)(g-1)\rangle^f\frac{\partial\langle T\rangle^f}{\partial x},\end{aligned} \tag{5.2}$$

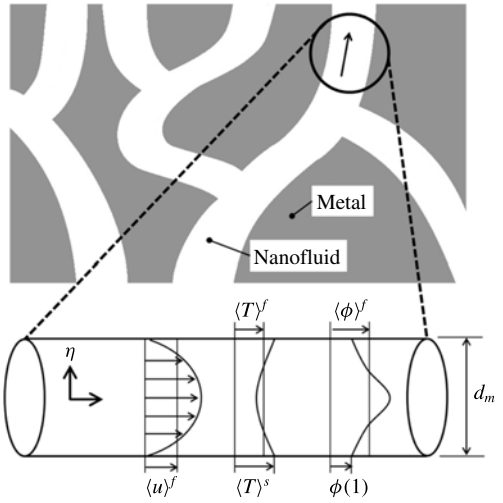

FIGURE 2. Pore-scale passage consideration; and pore-scale distributions of velocity, temperature and nanoparticles.

where the volume-averaged temperature difference between the two phases has been replaced by the volume-averaged temperature gradient, exploiting the foregoing macroscopic equation (5.1). Hence,

$$-\varepsilon\rho c\langle\tilde{T}\tilde{u}\rangle^f = \varepsilon k_{dis_{xx}}\frac{\partial\langle T\rangle^f}{\partial x}, \tag{5.3}$$

where

$$\varepsilon k_{dis_{xx}} = \frac{(\rho c\langle u\rangle)^2}{h_v}\langle(f-1)(g-1)\rangle^f, \tag{5.4}$$

which is consistent with what is known as the gradient diffusion hypothesis (Nakayama, Kuwahara & Kodama 2006). For the volumetric interstitial heat transfer coefficient h_v in (5.4), the following empirical correlation proposed by Calmidi & Mahajan (2000) may be used:

$$Nu_v = \frac{h_v d_m^2}{k_f} = 8.72(1-\varepsilon)^{1/4}\left(\frac{1-\mathrm{e}^{-(1-\varepsilon)/0.04}}{\varepsilon}\right)^{1/2}\left(\frac{\langle u\rangle d_m}{\nu}\right)^{1/2} Pr^{0.37}, \tag{5.5}$$

where d_m is the pore diameter. The correlation is based on the one developed by Zhukauskas (1987) for cylinders in laminar cross-flow. Note that the functions $f(\eta)$ and $g(\eta)$ describe the velocity and temperature profiles, respectively, in a pore passage of diameter d_m as illustrated in figure 2,

$$u = \langle u\rangle^f f(\eta) \tag{5.6a}$$

and

$$T - \langle T\rangle^s = (\langle T\rangle^f - \langle T\rangle^s)g(\eta), \tag{5.6b}$$

where the dimensionless radial coordinate η normal to the pore wall is defined as

$$\eta = 2r/d_m. \tag{5.7}$$

Any reasonable functions may be used for $f(\eta)$ and $g(\eta)$ in (5.4) to estimate $k_{dis_{xx}}$, such as laminar fully developed velocity and temperature profiles in a tube with diameter d_m:

$$f(\eta) = 2(1-\eta^2) \tag{5.8a}$$

and

$$g(\eta) = \tfrac{3}{4}(3-4\eta^2+\eta^4). \tag{5.8b}$$

Note that $\langle f(\eta)\rangle^f = \int_0^1 2\eta f(\eta)\mathrm{d}\eta = 1$ and $\langle g(\eta)\rangle^f = \int_0^1 2\eta g(\eta)\mathrm{d}\eta = 1$. Substituting the foregoing profiles into (5.4) along with (5.5), we readily obtain:

Longitudinal (laminar)

$$\begin{aligned}\frac{\varepsilon k_{dis_{xx}}}{k} &= \frac{(\rho c\langle u\rangle)^2}{h_v k}\langle (f-1)(g-1)\rangle^f = \frac{3}{8Nu_v}\left(\frac{\rho c\langle u\rangle d_m}{k}\right)^2 \\ &= \frac{3}{8}\frac{\left(\dfrac{\rho c\langle u\rangle d_m}{k}\right)^{3/2} Pr^{0.13}}{8.72(1-\varepsilon)^{1/4}\left(\dfrac{1-\mathrm{e}^{-(1-\varepsilon)/0.04}}{\varepsilon}\right)^{1/2}}.\end{aligned} \tag{5.9}$$

A similar relationship can be derived for the transverse thermal dispersion. We consider the energy equation (4.9) close enough to a heated wall surface for convection to be negligible, but sufficiently far away from the wall surface that transverse thermal dispersion dominates over stagnant thermal diffusion:

$$\varepsilon k_{dis_{yy}}\frac{\mathrm{d}^2\langle T\rangle^f}{\mathrm{d}r^2} \cong h_v(\langle T\rangle^f - \langle T\rangle^s), \tag{5.10}$$

which may be integrated to yield

$$\frac{\mathrm{d}\langle T\rangle^f}{\mathrm{d}r} = -\sqrt{\frac{h_v}{\varepsilon k_{dis_{yy}}}}\,(\langle T\rangle^f - \langle T\rangle^s) \tag{5.11}$$

such that

$$\begin{aligned}-\varepsilon\rho c_p\langle\tilde{v}\tilde{T}\rangle^f &\equiv \varepsilon k_{dis_{yy}}\frac{\mathrm{d}\langle T\rangle^f}{\mathrm{d}r} = -\rho c_p\langle u\rangle(\langle T\rangle^f - \langle T\rangle^s)\langle F(g-1)\rangle^f \\ &= \rho c_p\langle u\rangle\sqrt{\frac{\varepsilon k_{dis_{yy}}}{h_v}}\langle F(g-1)\rangle^f\frac{\mathrm{d}\langle T\rangle^f}{\mathrm{d}r}.\end{aligned} \tag{5.12}$$

Hence,

$$\varepsilon k_{dis_{yy}} = \frac{(\rho c\langle u\rangle)^2}{h_v}(\langle F(g-1)\rangle^f)^2, \tag{5.13}$$

where

$$v = \tilde{v} = \langle u\rangle^f F(\eta), \tag{5.14}$$

such that $\langle F(\eta)\rangle^f = \langle v\rangle^f/\langle u\rangle^f = 0$. Equation (5.13) obtained for the transverse thermal dispersion conductivity is the same as (5.4) obtained for the longitudinal thermal dispersion conductivity, except for the difference in the multiplicative constants, namely, $(\langle F(g-1)\rangle^f)^2$ and $\langle (f-1)(g-1)\rangle^f$. It is understood that $|F(\eta)| \ll 1$. In fact, the experimental data on a packed bed reported by Fried & Combarnous (1971)

suggest that $(\langle F(g-1)\rangle^f)^2$ is much smaller than $\langle (f-1)(g-1)\rangle^f$. In this study, we assume $\langle F(g-1)\rangle^f \cong \langle (f-1)(g-1)\rangle^f/15$, such that we obtain:

Transverse (laminar)

$$\begin{aligned}\frac{\varepsilon k_{dis_{yy}}}{k} &= \frac{(\rho c\langle u\rangle)^2}{h_v k}(\langle F(g-1)\rangle^f)^2 \\ &= \frac{3}{15^2\times 8}\frac{\left(\dfrac{\rho c\langle u\rangle d_m}{k}\right)^{3/2} Pr^{0.13}}{8.72(1-\varepsilon)^{1/4}\left(\dfrac{1-\mathrm{e}^{-(1-\varepsilon)/0.04}}{\varepsilon}\right)^{1/2}} \\ &= 0.00153\frac{\left(\dfrac{\rho c\langle u\rangle d_m}{k}\right)^{3/2} Pr^{0.13}}{(1-\varepsilon)^{1/4}\left(\dfrac{1-\mathrm{e}^{-(1-\varepsilon)/0.04}}{\varepsilon}\right)^{1/2}}.\end{aligned} \tag{5.15}$$

A similar procedure can be followed to estimate the longitudinal thermal dispersion for the case of fully turbulent flow, using the wall laws as

$$u = u_\tau\left(\frac{1}{\kappa}\ln n^+ + B\right) \tag{5.16a}$$

and

$$T - \langle T\rangle^s = -\frac{q_w\sigma_T}{u_\tau\rho_f c_{pf}}\left(\frac{1}{\kappa}\ln n^+ + A\right), \tag{5.16b}$$

where u_τ and q_w are friction velocity and wall heat flux, respectively, and $n^+ = u_\tau n/\nu$ is a dimensionless distance measured from the wall surface ($n = (d_m - 2r)/2$). Moreover, κ is the von Kármán constant, while B and A are both empirical constants. It is easy to find

$$\tilde{u} = \frac{u_\tau}{\kappa}\left(\ln\varsigma + \frac{3}{2}\right) \tag{5.17a}$$

and

$$\tilde{T} = -\frac{q_w\sigma_T}{u_\tau\rho c\kappa}\left(\ln\varsigma + \frac{3}{2}\right), \tag{5.17b}$$

where

$$\varsigma = 1 - \eta. \tag{5.18}$$

Hence

$$\begin{aligned}-\varepsilon\rho c\langle\tilde{T}\tilde{u}\rangle^f &= \varepsilon k_{dis_{xx}}\frac{\partial\langle T\rangle^f}{\partial x} = \frac{q_w\sigma_T}{\kappa^2}\left\langle\left(\ln\varsigma + \frac{3}{2}\right)^2\right\rangle^f \\ &= \frac{\sigma_T}{\kappa^2}\left\langle\left(\ln\varsigma + \frac{3}{2}\right)^2\right\rangle^f \frac{\rho c\langle u\rangle}{a_f}\frac{\mathrm{d}\langle T\rangle^f}{\mathrm{d}x} \\ &= \frac{\sigma_T}{4\varepsilon\kappa^2}\left(\frac{5}{4}\right)\rho c\langle u\rangle d_m\frac{\mathrm{d}\langle T\rangle^f}{\mathrm{d}x},\end{aligned} \tag{5.19}$$

where we have used (5.1) to eliminate the wall heat flux $q_w = -(h_v/a_f)(\langle T\rangle^f - \langle T\rangle^s)$ with specific surface $a_f = 4\varepsilon/d_m$ in favour of the temperature gradient. Setting κ and σ_T to 0.41 and 0.9, respectively, according to Launder & Spalding (1974), for the turbulent regime we obtain:

Longitudinal (turbulent)

$$\frac{\varepsilon k_{dis_{xx}}}{k} = \frac{\sigma_T}{4\varepsilon\kappa^2}\left(\frac{5}{4}\right)\frac{\rho c\langle u\rangle d_m}{k} = \frac{1.67}{\varepsilon}\left(\frac{\rho c\langle u\rangle d_m}{k}\right). \tag{5.20}$$

Taylor (1954) also assumed the law of the wall to explain the high-Péclet-number dependence observed in the dispersion of matter in pipe flow. The same linear relationship between the thermal dispersion conductivity and Péclet number may easily be deduced using an interstitial heat transfer coefficient correlation that increases linearly with Péclet number, as observed experimentally and explained theoretically by Nakayama *et al.* (2009) for high-Péclet-number flow through a consolidated porous medium.

As for the transverse dispersion, we again assume $k_{dis_{yy}} \equiv 15^2 k_{dis_{xx}}$, such that:

Transverse (turbulent)

$$\frac{\varepsilon k_{dis_{yy}}}{k} = \frac{\sigma_T}{4\varepsilon\kappa^2}\left(\frac{5}{4}\right)\frac{\rho c\langle u\rangle d_m}{k} = \frac{1.67}{15^2\varepsilon}\left(\frac{\rho c\langle u\rangle d_m}{k}\right) = \frac{0.00742}{\varepsilon}\left(\frac{\rho c\langle u\rangle d_m}{k}\right). \tag{5.21}$$

As for experimental data on metal foams, only those for transverse thermal dispersion are available. The data for transverse dispersion coefficient have been correlated by Calmidi & Mahajan (2000) as follows:

Transverse (Calmidi–Mahajan)

$$\frac{\varepsilon k_{dis_{yy}}}{k} = 0.00162\frac{\left(\dfrac{\rho c\langle u\rangle d_m}{k}\right)}{\left((1-\varepsilon)^{0.224}\left(\dfrac{1.18}{1-\mathrm{e}^{-(1-\varepsilon)/0.04}}\sqrt{\dfrac{1-\varepsilon}{3\pi}}\right)^{1.11}\right)^{1/2}}. \tag{5.22}$$

Thus, in figure 3, (5.15) obtained for the laminar case and (5.21) obtained for the turbulent case are presented together to form a solid curve for the case of $\varepsilon = 0.95$. In the figure, the foregoing empirical correlation (5.22) is also plotted to examine the validity of the present expressions for the transverse dispersion coefficient. The figure indicates fairly good agreement between the solid curve based on the present analysis and the dashed empirical line reported by Calmidi & Mahajan (2000). It should be noted that Calmidi & Mahajan's correlation is valid only when the Péclet number $(\rho c\langle u\rangle d_m/k)$ is sufficiently large, as we can conclude from the study of Taylor (1953). He analytically proved that the dispersion coefficient is proportional to $(\rho c\langle u\rangle d_m/k)^2$, that is consistent with our (5.9) for the case of small Péclet number, in which the interstitial heat transfer coefficient remains constant. It is also interesting to note that Gelhar & Carl (1983) and Wang & Kitanidis (1999) investigated macrodispersion in heterogeneous porous media such as aquifers and geological formations, in which they reported a Péclet-number dependence similar to what is observed in figure 3. Moreover, Ohsawa (2015) in his MS thesis carried out direct numerical simulations for nanofluid forced convection using a numerically generated periodic open cell. The thermal dispersion numerically predicted by him closely follows the empirical correlation (5.22) up to a Péclet number of 10 000, or even more.

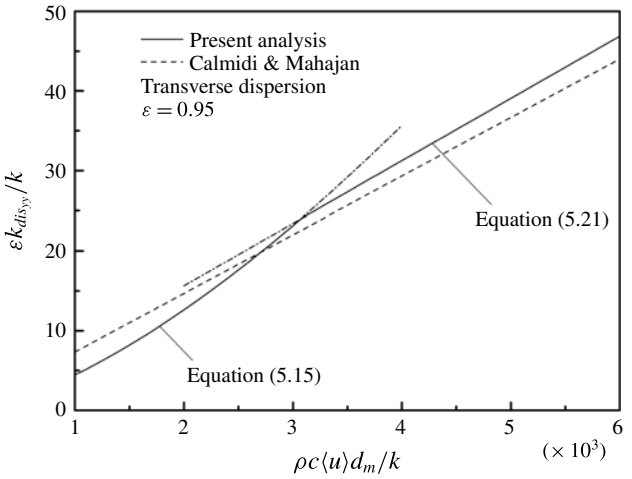

FIGURE 3. Transverse thermal dispersion in a nanofluid-saturated metal foam; a comparison of empirical correlation and present formulas.

Therefore, the empirical correlation (5.22) may well be valid in the range indicated in figure 3.

6. Nanoparticle mechanical dispersion

In what follows, we shall introduce a mathematical model for nanoparticle mechanical dispersion, for the first time. Along the macroscopic flow direction x, the nanoparticle conservation (4.11) at steady state may be written as

$$\frac{\partial \langle u\rangle \langle \phi\rangle^f}{\partial x} = \frac{\partial}{\partial x}\left(\varepsilon D_B \frac{\partial \langle \phi\rangle^f}{\partial x} + \frac{\varepsilon^* D_T}{\langle T\rangle^f}\frac{\partial \langle T\rangle^f}{\partial x} - \varepsilon \langle \tilde{\phi}\tilde{u}\rangle^f\right). \tag{6.1}$$

We again consider nanoparticle conservation along a pore-scale conduit with diameter d_m, as illustrated in figure 2. Thus, the nanoparticle mechanical dispersion flux $-\varepsilon\langle\tilde{\phi}\tilde{u}_j\rangle^f$ can be expressed as

$$-\varepsilon \langle \tilde{\phi}\tilde{u}\rangle^f = -\langle u\rangle \langle \phi\rangle^f \langle (f-1)(G-1)\rangle^f, \tag{6.2}$$

where

$$\phi = \langle \phi\rangle^f G(\eta). \tag{6.3}$$

The function $G(\eta)$ for the nanoparticle profile may be estimated by solving (2.4) in a pore conduit:

$$D_B \frac{\mathrm{d}\phi}{\mathrm{d}r} + \frac{D_T}{T}\frac{\mathrm{d}T}{\mathrm{d}r} = 0, \tag{6.4}$$

which can easily be solved with (2.6*a*) and (2.6*b*) being substituted:

$$\frac{\phi(\eta)}{\phi(1)} = \exp\left(\left.\frac{D_T}{\phi D_B}\right|_{\eta=1}\left(\frac{\langle T\rangle^s}{T(\eta)} - 1\right)\right) \cong 1 + \frac{\langle T\rangle^s - \langle T\rangle^f}{\langle T\rangle^s}\left.\frac{D_T}{\phi D_B}\right|_{\eta=1} g(\eta), \tag{6.5}$$

since $(\langle T\rangle^s - \langle T\rangle^f)/\langle T\rangle^s \ll 1$. Thus,

$$G(\eta) = \frac{\phi(1)}{\langle\phi\rangle^f}\left(1 + \frac{\langle T\rangle^s - \langle T\rangle^f}{\langle T\rangle^s}\left.\frac{D_T}{\phi D_B}\right|_{\eta=1} g(\eta)\right) = \frac{1 + \dfrac{\langle T\rangle^s - \langle T\rangle^f}{\langle T\rangle^s}\left.\dfrac{D_T}{\phi D_B}\right|_{\eta=1} g(\eta)}{1 + \dfrac{\langle T\rangle^s - \langle T\rangle^f}{\langle T\rangle^s}\left.\dfrac{D_T}{\phi D_B}\right|_{\eta=1}}. \tag{6.6}$$

Using (5.8*a*) and (5.8*b*) for the velocity and temperature profiles, respectively, we readily obtain

$$\langle (f-1)(G-1)\rangle^f = \frac{3}{8(1+n_{BT})} \cong \frac{3}{8n_{BT}}. \tag{6.7}$$

Thus

$$-\varepsilon\langle\tilde{\phi}\tilde{u}\rangle^f = -\frac{3}{8n_{BT}}\langle u\rangle\langle\phi\rangle^f, \tag{6.8}$$

where

$$n_{BT}(\langle T\rangle^f, \langle T\rangle^s) = \frac{\langle T\rangle^s}{\langle T\rangle^s - \langle T\rangle^f}\left.\frac{\phi D_B}{D_T}\right|_{\eta=1} \tag{6.9}$$

is a dimensionless function of local volume-averaged temperatures, describing the ratio of Brownian and thermophoretic diffusions within a pore conduit, as introduced by Yang *et al.* (2013*b*). Note that the absolute value of n_{BT} in most cases is very large, and that, under local thermal equilibrium condition, namely, $\langle T\rangle^s = \langle T\rangle^f$, it grows to infinity. Equation (6.8) may be substituted into (6.1) to yield

$$\frac{\partial\langle u\rangle\langle\phi\rangle^f}{\partial x} \cong \frac{1}{1+\dfrac{3}{8n_{BT}}}\frac{\partial}{\partial x}\left(\varepsilon D_B\frac{\partial\langle\phi\rangle^f}{\partial x} + \frac{\varepsilon^* D_T}{\langle T\rangle^f}\frac{\partial\langle T\rangle^f}{\partial x}\right). \tag{6.10}$$

It is interesting to note that the nanoparticle mechanical dispersion works either to suppress or to enhance the effective diffusion, as can be seen from the denominator $(1 + 3/8n_{BT})$. Where the local temperature of the metal foam phase is higher than that of the nanofluid phase (i.e. $n_{BT} > 0$), it suppresses the effective diffusion. On the other hand, where the local temperature of the metal foam phase is lower than that of the nanofluid phase (i.e. $n_{BT} < 0$), it enhances the diffusion. However, this effect of nanoparticle mechanical dispersion on the effective diffusion is limited only to a moderate range of n_{BT}, where local thermal non-equilibrium is discernible. In the region where n_{BT} is very large under nearly local thermal equilibrium, the nanoparticle mechanical dispersion flux $-\varepsilon\langle\tilde{\phi}\tilde{u}\rangle^f$ vanishes, and only stagnant particle diffusion remains. Thus, the nanoparticle mechanical dispersion flux varies across the channel, depending on the degree of local thermal non-equilibrium there.

We shall again consider the nanoparticle conservation (4.11) close enough to the wall surface for convection to be negligible:

$$\frac{\partial}{\partial y}\left(\varepsilon D_B\frac{\partial\langle\phi\rangle^f}{\partial y} + \frac{\varepsilon^* D_T}{\langle T\rangle^f}\frac{\partial\langle T\rangle^f}{\partial y} - \varepsilon\langle\tilde{\phi}\tilde{v}\rangle^f\right) \cong \frac{\partial}{\partial y}\left(\varepsilon D_B\frac{\partial\langle\phi\rangle^f}{\partial y} + \frac{\varepsilon^* D_T}{\langle T\rangle^f}\frac{\partial\langle T\rangle^f}{\partial y}\right) \cong 0. \tag{6.11}$$

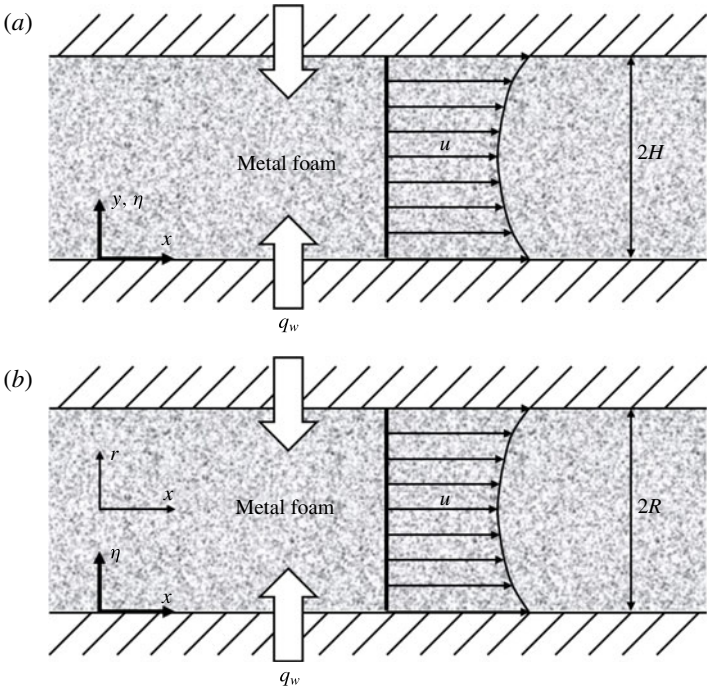

FIGURE 4. Fully developed flow subject to constant heat flux in (*a*) channel and (*b*) tube. Hydrodynamically and thermally fully developed flow is established in a channel/tube subject to constant heat flux, filled with a nanofluid-saturated metal foam, where the Darcian velocity is higher close to the wall since the viscosity there is lower.

The nanoparticle mechanical dispersion flux $-\varepsilon\langle\tilde{\phi}\tilde{v}\rangle^f$ near the wall surface may be estimated as follows:

$$-\varepsilon\langle\tilde{\phi}\tilde{v}\rangle^f = -\varepsilon\langle\tilde{\phi}\tilde{u}\rangle^f \frac{\langle F(G-1)\rangle^f}{\langle (f-1)(G-1)\rangle^f} \sim \frac{\langle u\rangle\langle\phi\rangle^f}{120 n_{BT}}. \tag{6.12}$$

Thus, the transverse nanoparticle mechanical dispersion is so small that it can be totally neglected, irrespective of the degree of local thermal non-equilibrium. Owing to the no-flux condition at the wall, (6.11) naturally reduces to

$$\varepsilon D_B \frac{\partial\langle\phi\rangle^f}{\partial y} + \frac{\varepsilon^* D_T}{\langle T\rangle^f}\frac{\partial\langle T\rangle^f}{\partial y} = 0. \tag{6.13}$$

Unfortunately, no experimental data are available for either transverse or longitudinal coefficients of nanoparticle mechanical dispersion.

7. Mathematical model for hydrodynamically and thermally fully developed flows

Referring to figure 4, we consider hydrodynamically and thermally fully developed flows in both channel and tube subject to constant heat flux, filled with a nanofluid-saturated metal foam. To be more precise, they are under axially constant heat flux and circumferentially constant wall temperature (i.e. constant heat flux everywhere). As will be revealed in the analysis, the Darcian velocity is higher close to the wall

since the viscosity there is lower. For this case of channel flow, the volume average equations (4.7)–(4.11) reduce to

$$-\frac{\mathrm{d}\langle p\rangle^f}{\mathrm{d}x}=\frac{\mu_f}{K}\langle u\rangle+\rho b\langle u\rangle^2, \tag{7.1}$$

$$\rho c\langle u\rangle\frac{\partial\langle T\rangle^f}{\partial x}=\frac{\partial}{\partial y}(\varepsilon^* k_f+\zeta_k\rho c d_m\langle u\rangle)\frac{\partial\langle T\rangle^f}{\partial y}-h_v(\langle T\rangle^f-\langle T\rangle^s), \tag{7.2}$$

$$\frac{\partial}{\partial y}(1-\varepsilon^*)k_s\frac{\partial\langle T\rangle^s}{\partial y}-h_v(\langle T\rangle^s-\langle T\rangle^f)=0, \tag{7.3}$$

$$\frac{\partial}{\partial y}\left(\varepsilon D_B\frac{\partial\langle\phi\rangle^f}{\partial y}+\frac{\varepsilon^* D_T}{\langle T\rangle^f}\frac{\partial\langle T\rangle^f}{\partial y}\right)=0. \tag{7.4}$$

Following (5.21), the transverse thermal dispersion coefficient may be evaluated from

$$\zeta_k=\frac{0.00742}{\varepsilon}. \tag{7.5}$$

Moreover, the interstitial volumetric coefficient h_v is evaluated from (5.5). Note that the continuity equation yields $\partial\langle u\rangle/\partial x=0$ and $\langle v\rangle=0$. The momentum equation (4.8) is simplified using the Forchheimer-extended Darcy law, in which the Brinkman term (i.e. macroscopic viscous diffusion term) is dropped. This Forchheimer-extended Darcy law is valid for most metal foams except for the case of extremely high permeability.

The origin of vertical coordinate y is set on the lower wall. The boundary conditions are given by

$$q_0=-(\varepsilon^* k_f+\zeta_k\rho c d_m\langle u\rangle)\left.\frac{\partial\langle T\rangle^f}{\partial y}\right|_{y=0}-(1-\varepsilon^*)k_s\left.\frac{\partial\langle T\rangle^s}{\partial y}\right|_{y=0}, \tag{7.6}$$

$$\left.\varepsilon D_B\frac{\partial\langle\phi\rangle^f}{\partial y}\right|_{y=0}+\left.\frac{\varepsilon^* D_T}{\langle T\rangle^f}\frac{\partial\langle T\rangle^f}{\partial y}\right|_{y=0}=0, \tag{7.7}$$

$$\left.\frac{\partial\langle\phi\rangle^f}{\partial y}\right|_{y=H}=0,\qquad\left.\frac{\partial\langle T\rangle^f}{\partial y}\right|_{y=H}=\left.\frac{\partial\langle T\rangle^s}{\partial y}\right|_{y=H}=0. \tag{7.8a,b}$$

Kuwahara *et al.* (2011) considered two extreme cases for possible wall temperature difference between solid and fluid phases, namely, locally uniform heat flux wall and locally thermal equilibrium wall, and concluded that the locally thermal equilibrium wall is much closer to reality. Hence, we assume

$$\langle T\rangle^s|_{y=0}=\langle T\rangle^f|_{y=0}\equiv T_0(x), \tag{7.9}$$

where $T_0(x)$ is the wall temperature, which increases linearly downstream under constant heat flux. The nanoparticle conservation equation (7.4) indicates that the diffusion mass flux of nanoparticles is constant across the channel. Since the wall is impermeable, the boundary condition (7.7) holds such that the effective Brownian diffusion flux and the effective thermophoretic diffusion flux cancel out everywhere across the channel. Energy equations (7.2) and (7.3) may be added and integrated over the lower half-channel from $y=0$ to H with boundary conditions (7.6) and (7.7) to give

$$\overline{\rho c\langle u\rangle}\frac{\mathrm{d}T_B}{\mathrm{d}x}=\frac{q_0}{H}, \tag{7.10}$$

where the subscript 0 refers to the wall at $y = 0$, and

$$\overline{\varphi} \equiv \frac{1}{A}\int_A \varphi \mathrm{d}A = \frac{1}{H}\int_0^H \varphi \mathrm{d}y \tag{7.11}$$

denotes the average value over the cross-section such that

$$T_B \equiv \frac{\overline{\rho c \langle u\rangle \langle T\rangle}}{\overline{\rho c \langle u\rangle}} \tag{7.12a}$$

is the bulk mean temperature. Likewise, quantities with subscript B denote bulk quantities such as

$$\phi_B \equiv \overline{\langle u\rangle \langle \phi\rangle^f}/\overline{\langle u\rangle}, \quad u_B \equiv \overline{\rho\langle u\rangle}/\rho(\phi_B). \tag{7.12b,c}$$

The foregoing considerations on both the nanoparticle diffusion flux and axial temperature gradient will be implemented to obtain analytical expressions in dimensionless form. The momentum equation (7.1) may be arranged in a dimensionless form as

$$u^*(y^*) = \frac{\sqrt{1 + 4\,Da^2 Hg \dfrac{(\rho/\rho_0)}{(\mu/\mu_0)^2}} - 1}{2\,Da\,Hg\dfrac{(\rho/\rho_0)}{(\mu/\mu_0)}}. \tag{7.13}$$

Thus, for the case of the Forchheimer-extended Darcy flow (i.e. $Da \ll 1$), the velocity profile is described algebraically as the viscosity of the nanofluid is provided as a function of the nanoparticle volume fraction. The other governing equations are given in differential forms as follows:

$$\frac{\rho c u^*}{\overline{\rho c u^*}} = -\frac{\mathrm{d}}{\mathrm{d}y^*}\left(\varepsilon^* \frac{k}{k_{stag0}} + \zeta_k\, Pe \frac{\rho c}{(\rho c)_0} u^*\right)\frac{\mathrm{d}T^{*f}}{\mathrm{d}y^*} + Nu_v(T^{*f} - T^{*s}), \tag{7.14}$$

$$(1-\varepsilon^*)\frac{k_s}{k_{stag0}}\frac{\mathrm{d}^2 T^{*s}}{\mathrm{d}y^{*2}} - Nu_v(T^{*s} - T^{*f}) = 0, \tag{7.15}$$

$$\frac{\mathrm{d}\langle\phi\rangle^f}{\mathrm{d}y^*} = \frac{\varepsilon^*\langle\phi\rangle^f}{\varepsilon N_{BT}(1-\gamma T^{*f})^2}\frac{\mathrm{d}T^{*f}}{\mathrm{d}y^*}. \tag{7.16}$$

The dimensionless coordinate, velocity and temperature are defined as

$$y^* = y/H, \tag{7.17}$$

$$u^* = \langle u\rangle \Big/ \left(\frac{H^2}{\mu_0}\left(-\frac{\mathrm{d}\langle p\rangle^f}{\mathrm{d}x}\right)\right), \tag{7.18a}$$

$$T^{*f} = \frac{k_{stag0}(T_0 - \langle T\rangle^f)}{q_0 H}, \tag{7.18b}$$

$$T^{*s} = \frac{k_{stag0}(T_0 - \langle T\rangle^s)}{q_0 H}, \tag{7.18c}$$

$$N_{BT} \equiv \frac{D_{B0} T_0 \phi_0 k_{stag0}}{D_{T0} q_0 H} = \frac{D_{B0} \phi_0}{D_{T0} \gamma}, \tag{7.19a}$$

$$\gamma \equiv \frac{q_0 H}{k_{stag0} T_0}. \tag{7.19b}$$

Furthermore, the Darcy, Lewis, Péclet and Hagen numbers are defined as follows:

$$Da \equiv K/H^2, \tag{7.20a}$$

$$Le \equiv k_{stag0}/(\rho c)_0 D_{B0}, \tag{7.20b}$$

$$Pe \equiv \frac{\rho_0 c_0 \sqrt{K}}{k_{stag0}} \frac{H^2}{\mu_0} \left(-\frac{\mathrm{d}\langle p \rangle^f}{\mathrm{d}x} \right), \tag{7.20c}$$

$$Hg \equiv \frac{\rho_0 b H^4}{\mu_0^2} \left(-\frac{\mathrm{d}\langle p \rangle^f}{\mathrm{d}x} \right), \tag{7.20d}$$

where the properties with subscript 0 should be evaluated at the wall according to (2.5*a*)–(2.6*b*), (4.4) and (4.5). For example, the stagnation thermal conductivity at the wall where $\langle \phi \rangle^f|_{y^*=0} = \phi_0$ may be evaluated according to (2.5*d*), (4.4) and (4.5) as

$$k_{stag0} = \varepsilon^* k|_{y^*=0} + (1-\varepsilon^*) k_s = \frac{2+\varepsilon}{3}(1 + 2.72\phi_0 + 4.97\phi_0^2) k_{bf} + \frac{1-\varepsilon}{3} k_s. \tag{7.21}$$

The dimensionless parameter N_{BT} is the ratio of macroscopic Brownian and thermophoretic diffusivities, which can range over a wide range from 0.1 to 10 for typical cases of alumina and copper nanoparticles with $d_p \sim 10$ nm and the bulk mean particle volume fraction $\phi_B \sim 0.01$, while the ratio of wall and fluid temperature difference to absolute temperature $\gamma \sim (T_0 - \langle T \rangle_B^f)/T_0$ is usually much smaller than unity, as estimated by Buongiorno (2006). The similarity between the 'microscopic' ratio n_{BT} (6.9) and the 'macroscopic' ratio N_{BT} (7.19*a*) is interesting, since the former describes the local ratio of microscopic Brownian and thermophoretic diffusivities at pore scale, whereas the latter describes the ratio of macroscopic Brownian and thermophoretic diffusivities in a channel filled with a nanofluid-saturated metal foam.

In reality, the bulk mean particle volume fraction ϕ_B is prescribed instead of that at the wall ϕ_0. However, for the sake of computational convenience, ϕ_0 is prescribed and ϕ_B is calculated later to find ϕ_0 as a function of ϕ_B.

The energy equations (7.14) and (7.15) can be combined to form a third-order ordinary differential equation (ODE) with respect to T^{*s} as

$$\frac{\mathrm{d}^3 T^{*s}}{\mathrm{d}y^{*3}} = Nu_v \frac{\left(\dfrac{k_{stag}}{k_{stag0}} + \zeta_k Pe \dfrac{\rho c}{(\rho c)_0} u^* \right) \dfrac{\mathrm{d}T^{*s}}{\mathrm{d}y^*} - \displaystyle\int_\eta^1 \frac{\rho c u^*}{\overline{\rho c u^*}} \mathrm{d}y^*}{\left(\varepsilon^* \dfrac{k_f}{k_{stag0}} + \zeta_k Pe \dfrac{\rho c}{(\rho c)_0} u^* \right) (1-\varepsilon^*) \dfrac{k_s}{k_{stag0}}}, \tag{7.22}$$

where

$$T^{*f} = T^{*s} - \frac{(1-\varepsilon^*)}{Nu_v} \frac{k_s}{k_{stag0}} \frac{\mathrm{d}^2 T^{*s}}{\mathrm{d}y^{*2}} \tag{7.23}$$

and (7.16) can easily be integrated with $\langle \phi \rangle^f|_{y^*=0} = \phi_0$ to obtain

$$\frac{\langle \phi \rangle^f}{\phi_0} = \exp\left(\frac{\varepsilon^* T^{*f}}{N_{BT} \varepsilon (1 - \gamma T^{*f})} \right). \tag{7.24}$$

The foregoing third-order ODE (7.22) may easily be solved by using a standard integration scheme such as the Runge–Kutta–Gill method (e.g. Nakayama 1995). Appropriate boundary conditions for the equation are given by

$$T^{*s}|_{y^*=0} = \left.\frac{\mathrm{d}^2 T^{*s}}{\mathrm{d}y^{*2}}\right|_{y^*=0} = 0 \quad \text{and} \quad \left.\frac{\mathrm{d}T^{*s}}{\mathrm{d}y^*}\right|_{y^*=1} = 0, \tag{7.25a,b}$$

which are based on the original boundary conditions given by (7.8*b*) and (7.1).

A similar procedure based on the cylindrical coordinate system as shown in figure 3(*b*) readily yields the following set of transformed equations for the case of a circular tube:

$$\frac{\mathrm{d}^3 T^{*s}}{\mathrm{d}y^{*3}} - \frac{1}{1-y^*}\frac{\mathrm{d}^2 T^{*s}}{\mathrm{d}y^{*2}} - \frac{1}{(1-y^*)^2}\frac{\mathrm{d}T^{*s}}{\mathrm{d}y^*} = Nu_v \frac{\left(\dfrac{k_{stag}}{k_{stag0}} + \zeta_k\, Pe \dfrac{\rho_f c_f}{\rho_{f0} c_{f0}} u^*\right)\dfrac{\mathrm{d}T^{*s}}{\mathrm{d}y^*} - \dfrac{2}{1-y^*}\displaystyle\int_{y^*}^{1} \frac{\rho_f c_f u^*}{\overline{\rho c u^*}}(1-y^*)\mathrm{d}y^*}{\left(\varepsilon^* \dfrac{k_f}{k_{stag0}} + \zeta_k\, Pe \dfrac{\rho_f c_f}{\rho_{f0} c_{f0}} u^*\right)(1-\varepsilon^*)\dfrac{k_s}{k_{stag0}}}, \tag{7.26}$$

where

$$T^{*f} = T^{*s} - \frac{(1-\varepsilon^*)}{Nu_v}\frac{k_s}{k_{stag0}}\left(\frac{\mathrm{d}^2 T^{*s}}{\mathrm{d}y^{*2}} - \frac{1}{1-y^*}\frac{\mathrm{d}T^{*s}}{\mathrm{d}y^*}\right). \tag{7.27}$$

The boundary conditions in cylindrical coordinates are the same as those given by (7.25*a*,*b*). Moreover, (7.24) for the volume-averaged nanoparticle volume fraction holds also for the case of the cylindrical coordinate system. However, note that the average value $\bar{\varphi}$ for the case of the tube is computed by

$$\bar{\varphi} \equiv \frac{1}{A}\int_A \varphi \mathrm{d}A = \frac{1}{\pi R^2}\int_0^R 2\pi r \varphi \mathrm{d}r = 2\int_0^1 (1-y^*)\varphi \mathrm{d}y^*, \tag{7.28}$$

where $y^* = (R-r)/R$. The corresponding dimensionless quantities u^* to Nu_v are defined just as presented in (7.18*a*)–(7.20*d*) by replacing the channel half-height H by the tube radius R.

8. Results and discussion

The foregoing sets of equations are numerically integrated using the Runge–Kutta–Gill method for the case of a channel with $\varepsilon = 0.9$, $Da = 10^{-4}$, $N_{BT} = 0.5$ and $\phi_B = 0.02$. The effects of the interstitial Nusselt number Nu_v on the fluid and solid temperature profiles are illustrated in figure 5.

The temperature profiles of the nanofluid and the metal foam overlap each other for sufficiently large Nu_v, in which local thermal equilibrium holds. In general, the solid temperature is higher than the nanofluid temperature, i.e. $T^{*s} = k_{stag0}(T_0 - \langle T\rangle^s)/q_0 H$ is smaller and flatter than $T^{*f} = k_{stag0}(T_0 - \langle T\rangle^f)/q_0 H$.

Figures 6 and 7 show the corresponding particle volume fraction and velocity profiles in the channel, respectively. The nanoparticle volume fraction distribution becomes somewhat flatter for large Nu_v, since the nanofluid temperature tends to follow the solid temperature, as witnessed in figure 5. The nanoparticle volume

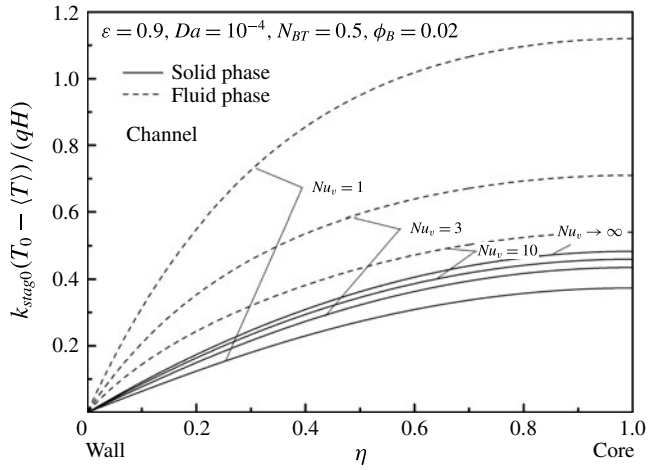

FIGURE 5. Effects of Nu_v on the temperature profiles in a channel filled with a nanofluid-saturated metal foam.

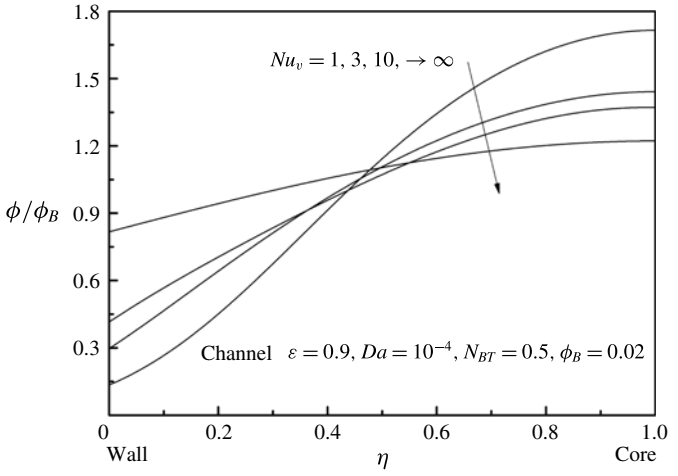

FIGURE 6. Effects of Nu_v on the nanoparticle distribution in a channel filled with a nanofluid-saturated metal foam.

fraction gradually converges to a profile corresponding to the case of $Nu_v \to \infty$. Figure 7 shows that the velocity is higher near the heated wall where the viscosity is less since thermophoretic diffusion dominates over Brownian diffusion, driving nanoparticles away from the wall.

Another series of computations were carried out with $\varepsilon = 0.9$, $Da = 10^{-4}$, $Nu_v = 1$ and $\phi_B = 0.02$, to investigate the effect of the ratio of macroscopic Brownian and thermophoretic diffusivities, N_{BT} on the nanoparticle volume fraction profile, velocity profile and both fluid and solid temperature profiles, by changing the value of N_{BT}.

Figure 8 indicates that the nanoparticle volume fraction becomes uniform on increasing N_{BT}. Since Brownian diffusion dominates over thermophoretic diffusion, nanoparticles tend to be dispersed evenly for large N_{BT}. Under such a uniform

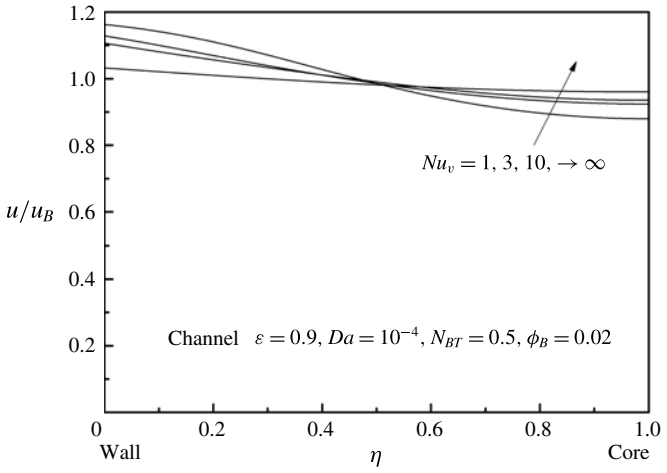

FIGURE 7. Effects of Nu_v on the velocity distribution in a channel filled with a nanofluid-saturated metal foam.

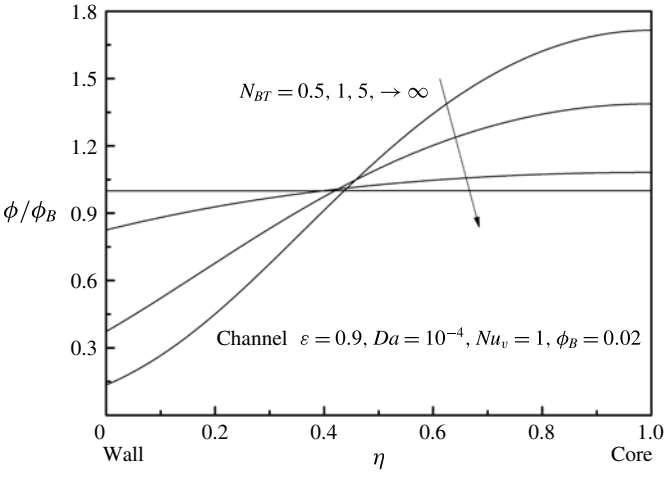

FIGURE 8. Effects of N_{BT} on the nanoparticle volume fraction distribution in a channel filled with a nanofluid-saturated metal foam.

nanoparticle volume fraction distribution, the velocity profile becomes completely flat, resulting in plug flow, as shown in figure 9.

In figure 10, both nanofluid temperature and metal foam temperature are presented for a range of N_{BT}. Since Nu_v is at a moderate level, a substantial difference can be observed between the two temperatures. The effects of N_{BT} on the temperature profiles, however, are rather limited, as can be confirmed from the figure.

8.1. *Asymptotic solutions for nearly uniform nanoparticle distribution* ($N_{BT} \gg 1$)

When the nanoparticle diameter is sufficiently small, Brownian diffusion overwhelms thermophoretic diffusion, and its macroscopic ratio N_{BT} remains much greater than

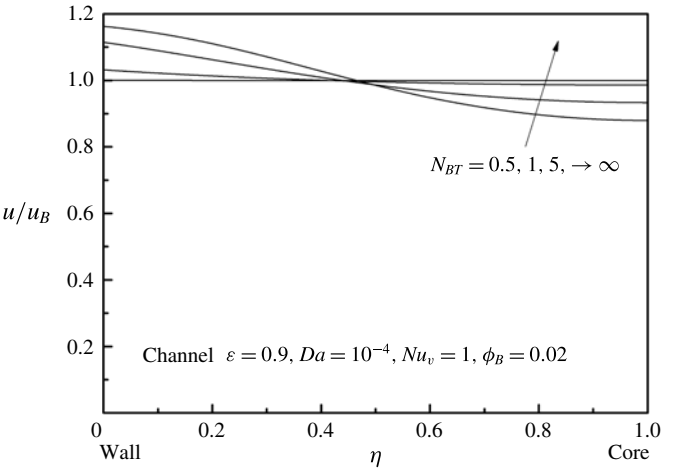

FIGURE 9. Effects of N_{BT} on the velocity distribution in a channel filled with a nanofluid-saturated metal foam.

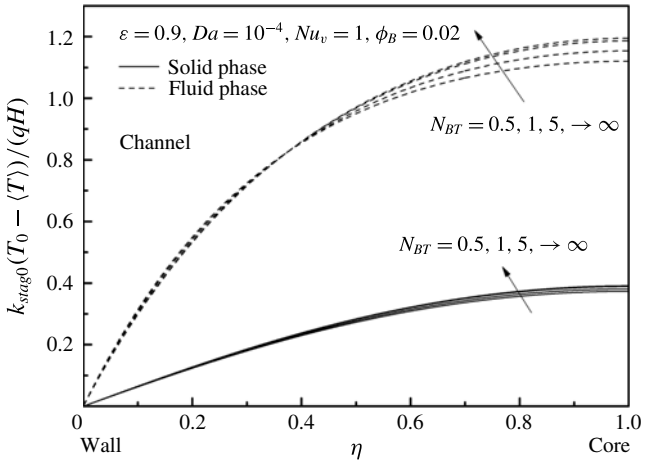

FIGURE 10. Effects of N_{BT} on the temperature distribution in a channel filled with a nanofluid-saturated metal foam.

unity. In such cases, (7.24) yields

$$\frac{\langle \phi \rangle^f}{\phi_0} = \exp\left(\frac{\varepsilon^* T^{*f}}{N_{BT}\varepsilon(1-\gamma T^{*f})}\right) \cong 1 + \frac{\varepsilon^*}{N_{BT}\varepsilon} T^{*f}, \tag{8.1}$$

where $\gamma \ll 1$. This equation reveals that the profile of the volume-averaged nanoparticle volume fraction $\langle \phi \rangle^f(y^*)$ is similar to that of the nanofluid phase temperature $T^{*f}(y^*)$. Moreover, it tends to be uniform for sufficiently large N_{BT}, as consistently observed in figure 8. Under such a uniform distribution of volume-averaged nanoparticle volume fraction, all thermophysical properties become uniform across the channel.

8.1.1. *Channel flows*

Thus, the third-order ODE (7.22) and the nanofluid temperature (7.23) with the boundary conditions (7.25*a*,*b*) yield the following analytic solutions:

$$T^{*s} = \frac{y^* - \frac{1}{2}y^{*2} - \frac{1}{\xi^2}\left(1 - \frac{\cosh(\xi(1-y^*))}{\cosh\xi}\right)}{1 + \zeta_k Pe\, u_B^*} \tag{8.2}$$

and

$$T^{*f} = \frac{y^* - \frac{1}{2}y^{*2} + \frac{1 - \varepsilon^* \frac{k(\phi_B)}{k_{stag0}}}{\left(\varepsilon^* \frac{k(\phi_B)}{k_{stag0}} + \zeta_k Pe\, u_B^*\right)\xi^2}\left(1 - \frac{\cosh(\xi(1-y^*))}{\cosh\xi}\right)}{1 + \zeta_k Pe\, u_B^*}, \tag{8.3}$$

where

$$\xi = \sqrt{\frac{1 + \zeta_k Pe\, u_B^*}{(1-\varepsilon^*)\frac{k_s}{k_{stag0}}\left(\varepsilon^* \frac{k(\phi_B)}{k_{stag0}} + \zeta_k Pe\, u_B^*\right)} Nu_v} \tag{8.4a}$$

and

$$u_B^* = \frac{\sqrt{1 + 4\,Da^2\,Hg} - 1}{2\,Da\,Hg}. \tag{8.4b}$$

The Nusselt number of interest is given by

$$\begin{aligned} Nu_H &= \frac{q_0 H}{k(\phi_B)(T_0 - T_B)} = \frac{1}{\frac{k(\phi_B)}{k_{stag0}} T_B^*} = \frac{1}{\frac{k(\phi_B)}{k_{stag0}} \overline{T^{*f}}} \\ &= \frac{k_{stag0}}{k(\phi_B)} \frac{1 + \zeta_k Pe\, u_B^*}{\frac{1}{3} + \frac{1 - \frac{2+\varepsilon}{3}\frac{k(\phi_B)}{k_{stag0}}}{\left(\frac{2+\varepsilon}{3}\frac{k(\phi_B)}{k_{stag0}} + \zeta_k Pe\, u_B^*\right)\xi^2}\left(1 - \frac{\tanh\xi}{\xi}\right)}. \end{aligned} \tag{8.5}$$

The ratio of heat transfer coefficient for convection in a nanofluid-saturated metal foam to that for the case of base fluid convection without a metal foam is given by

$$\frac{h(\phi_B)}{h_{bf}} = \frac{4}{140/17}\frac{k_{stag0}}{k_{bf}} \frac{1 + \zeta_k Pe\, u_B^*}{\frac{1}{3} + \frac{1 - \frac{2+\varepsilon}{3}\frac{k(\phi_B)}{k_{stag0}}}{\left(\frac{2+\varepsilon}{3}\frac{k(\phi_B)}{k_{stag0}} + \zeta_k Pe\, u_B^*\right)\xi^2}\left(1 - \frac{\tanh\xi}{\xi}\right)}. \tag{8.6}$$

8.1.2. *Tube flows*

The corresponding set of solutions for the case of tubes may be obtained by solving (7.26) as

$$T^{*s} = \frac{y^* - \frac{1}{2}y^{*2} - \frac{2}{\xi^2}\left(1 - \frac{\mathrm{I}_0(\xi(1-y^*))}{\mathrm{I}_0(\xi)}\right)}{1 + \zeta_k Pe\, u_B^*} \tag{8.7}$$

where I_0 is the modified zero-order Bessel function of the first kind. The dimensionless nanofluid temperature is obtained by substituting (8.7) into (7.27) as

$$T^{*f} = \frac{y^* - \frac{1}{2}y^{*2} + \frac{2\left(1 - \varepsilon^* \frac{k(\phi_B)}{k_{stag0}}\right)}{\left(\varepsilon^* \frac{k(\phi_B)}{k_{stag0}} + \zeta_k Pe\, u_B^*\right)\xi^2}\left(1 - \frac{\mathrm{I}_0(\xi(1-y^*))}{\mathrm{I}_0(\xi)}\right)}{1 + \zeta_k Pe\, u_B^*}, \tag{8.8}$$

where the dimensionless bulk velocity is given by (8.4*b*). The corresponding Nusselt number may be numerically evaluated as

$$Nu_R = \frac{q_0 R}{k(\phi_B)(T_0 - T_B)} = \frac{1}{\frac{k(\phi_B)}{k_{stag0}} T_B^*} = \frac{1}{\frac{k(\phi_B)}{k_{stag0}} \overline{T^{*f}}}. \tag{8.9}$$

The ratio of heat transfer coefficient for convection in a nanofluid-saturated metal foam to that for the case of base fluid convection without a metal foam is given by

$$\frac{h(\phi_B)}{h_{bf}} = \frac{2}{48/11} \frac{k_{stag0}}{k_{bf}} \frac{1}{\overline{T^{*f}}}. \tag{8.10}$$

8.2. *Asymptotic solutions for nearly local thermal equilibrium* ($Nu_v \gg 1$)

Equation (7.23) for the channel flow case and (7.27) for the tube flow case clearly indicate $T^{*f} \cong T^{*s}$ when the interstitial volumetric coefficient is sufficiently high (i.e. $Nu_v \gg 1$). Thus, local thermal equilibrium holds everywhere over the cross-section.

8.2.1. *Channel flows*

Equation (7.14) readily yields analytic solutions:

$$T^{*f} \cong T^{*s} = \int_0^{y^*} \frac{\int_{y^*}^1 \frac{\rho c u^*}{\overline{\rho c u^*}} \mathrm{d}y^*}{\frac{k_{stag}}{k_{stag0}} + \zeta_k Pe \left(\frac{\rho c}{\rho_0 c_0}\right) u^*} \mathrm{d}y^*. \tag{8.11}$$

This integral equation can be approximated very well by

$$T^{*f} \cong T^{*s} = \frac{y^* - \frac{1}{2}y^{*2}}{\frac{k_{stag}(\phi_B)}{k_{stag0}} + \zeta_k Pe \frac{\sqrt{1 + 4\,Da^2\,Hg} - 1}{2\,Da\,Hg}}. \tag{8.12}$$

Substitution of the foregoing temperature profile into (7.24) readily gives the profile of the volume-averaged nanoparticle volume fraction. The corresponding Nusselt number is given by

$$Nu_H = \frac{q_0 H}{k(\phi_B)(T_0 - T_B)} = \frac{1}{\dfrac{k(\phi_B)}{k_{stag0}} T_B^*} = \frac{1}{\dfrac{k(\phi_B)}{k_{stag0}} \overline{T^{*f}}}$$
$$= 3\left(1 + \frac{k_{stag0}}{k(\phi_B)} \zeta_k \, Pe \frac{\sqrt{1 + 4\,Da^2\,Hg} - 1}{2\,Da\,Hg}\right). \tag{8.13}$$

The ratio of heat transfer coefficient for convection in a nanofluid-saturated metal foam to that for the case of base fluid convection without a metal foam is given by

$$\frac{h(\phi_B)}{h_{bf}} = \frac{12}{140/17}\left(\frac{k(\phi_B)}{k_{bf}} + \frac{k_{stag0}}{k_{bf}} \zeta_k \, Pe \frac{\sqrt{1 + 4\,Da^2\,Hg} - 1}{2\,Da\,Hg}\right). \tag{8.14}$$

8.2.2. *Tube flows*

The corresponding set of solutions for the case of tubes may be obtained from (7.26) as

$$T^{*f} \cong T^{*s} = \int_0^{y^*} \frac{\displaystyle\int_{y^*}^1 2(1 - y^*) \frac{\rho c u^*}{\overline{\rho c u^*}} \mathrm{d}\eta}{(1 - y^*)\left(\dfrac{k_{stag}}{k_{stag0}} + \zeta_k \, Pe \left(\dfrac{\rho c}{\rho_0 c_0}\right) u^*\right)} \mathrm{d}y^*, \tag{8.15}$$

which may be approximated well by

$$T^{*f} \cong T^{*s} = \frac{y^* - \dfrac{1}{2} y^{*2}}{\dfrac{k_{stag}(\phi_B)}{k_{stag0}} + \zeta_k \, Pe \dfrac{\sqrt{1 + 4\,Da^2\,Hg} - 1}{2\,Da\,Hg}}. \tag{8.16}$$

Thus, the profile of volume-averaged temperature given by (8.16) and that of nanoparticle volume fraction given by its substitution into (7.24) for the tube are similar to those for the channel. Accordingly, the Nusselt number for the tube is given by

$$Nu_R = \frac{q_0 R}{k(\phi_B)(T_0 - T_B)} = \frac{1}{\dfrac{k(\phi_B)}{k_{stag0}} T_B^*} = \frac{1}{\dfrac{k(\phi_B)}{k_{stag0}} \overline{T^{*f}}}$$
$$= 4\left(1 + \frac{k_{stag0}}{k(\phi_B)} \zeta_k \, Pe \frac{\sqrt{1 + 4\,Da^2\,Hg} - 1}{2\,Da\,Hg}\right). \tag{8.17}$$

The ratio of heat transfer coefficient for convection in a nanofluid-saturated metal foam to that for the case of base fluid convection without a metal foam is given by

$$\frac{h(\phi_B)}{h_{bf}} = \frac{8}{48/11}\left(\frac{k_{stag}(\phi_B)}{k_{bf}} + \frac{k_{stag0}}{k_{bf}} \zeta_k \, Pe \frac{\sqrt{1 + 4\,Da^2\,Hg} - 1}{2\,Da\,Hg}\right). \tag{8.18}$$

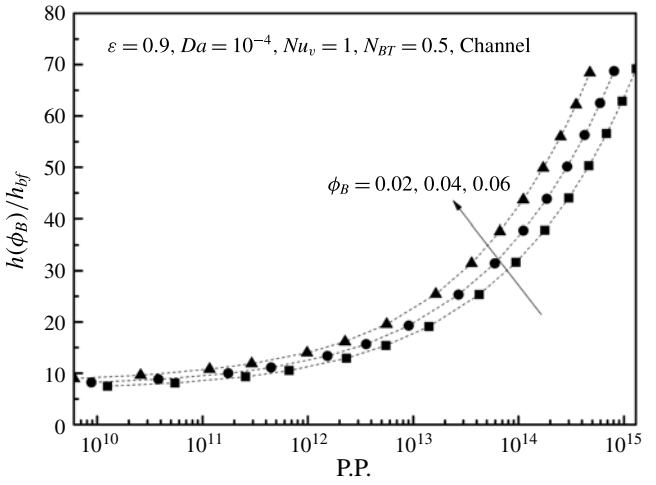

FIGURE 11. Effects of ϕ_B on the heat transfer coefficient ratio in a channel filled with a nanofluid-saturated metal foam.

Heat transfer enhancement in a nanoparticle-saturated metal foam can be partly attributed to an increase in its stagnant thermal conductivity, which results from both highly conductive nanoparticles and consolidated metal foam, and partly to intensified nanofluid mixing due to mechanical dispersion within the foam. This enhancement may best be illustrated in the foregoing (8.18). It should be noted that the first term on the right-hand side gives the heat transfer rate increase due to embedding of the metal foam and the addition of nanoparticles, whereas the second term describes heat transfer enhancement due to thermal dispersion.

8.3. *Heat transfer performance evaluation*

In figure 11, heat transfer coefficient ratios $h(\phi_B)/h_{bf}$ with given ϕ_B are presented versus the dimensionless pumping power,

$$\text{P.P.}(Hg;\, Da) \equiv \left(-\frac{\mathrm{d}\langle p\rangle^f}{\mathrm{d}x}u_B\right)\left(\frac{\rho_0^2 b^2 R^6}{\mu_0^3}\right) = \frac{\sqrt{1+4\,Da^2\,Hg}-1}{2Da}Hg, \tag{8.19}$$

in the possible range of P.P. $= 6.0 \times 10^9$ to 1.3×10^{15} (corresponding to $\langle u\rangle = 0.01$ to 1 m s^{-1}, $2R = 0.02$ m, $d_m = 0.001$ m) for the tube. The figure clearly shows that the heat transfer coefficient of a tube filled with a nanofluid-saturated metal foam is much higher than that of a tube filled with a base fluid. The ratio increases towards 80 with the pumping power P.P., as thermal dispersion becomes significant. Naturally, a higher volume fraction of nanofluid results in a higher heat transfer coefficient, especially when P.P. is large such that thermal dispersion is dominant.

The effects of N_{BT} on the heat transfer ratio $h(\phi_B)/h_{bf}$ are illustrated in figure 12. As expected from figure 10, showing the temperature profiles, which are fairly insensitive to N_{BT}, the heat transfer ratios obtained with different values of N_{BT} almost overlap one another. Figure 13, on the other hand, shows the effects of Nu_v on the heat transfer coefficient ratio $h(\phi_B)/h_{bf}$, which clearly indicates that higher interstitial heat transfer coefficient yields higher macroscopic heat transfer coefficient. Thus, the combination of metal foams and nanofluids results in unconventionally high heat transfer coefficients.

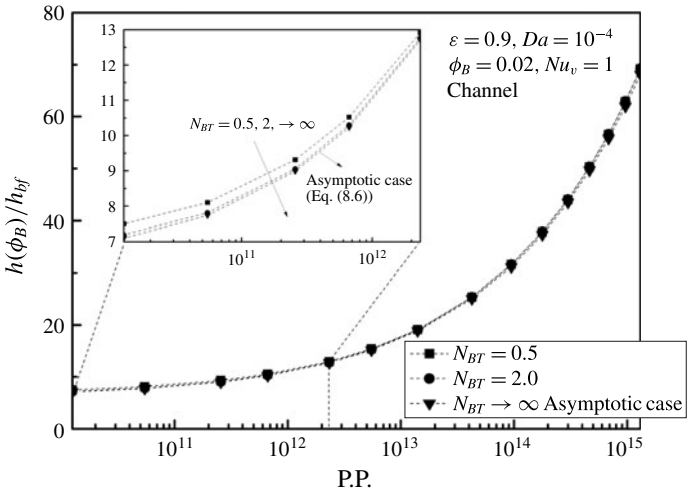

FIGURE 12. Effects of N_{BT} on the heat transfer coefficient ratio in a channel filled with a nanofluid-saturated metal foam.

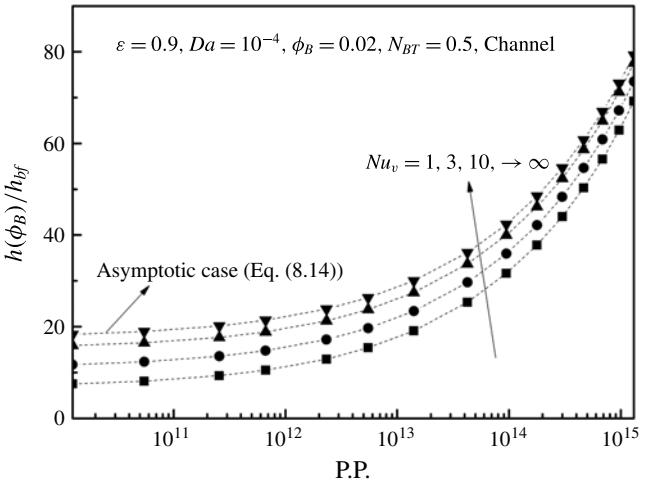

FIGURE 13. Effects of Nu_v on the heat transfer coefficient ratio in a channel filled with a nanofluid-saturated metal foam.

9. Conclusions

The set of macroscopic governing equations appropriate for convective heat transfer in a nanofluid-saturated metal foam were derived rigorously by applying a volume-averaging theory to the microscopic set of modified Buongiorno equations. Unknown terms are mathematically modelled so as to close the set of governing equations. Mechanical dispersion terms, namely, the thermal dispersion term and particle mechanical dispersion term, were considered analytically using a pore-scale conduit model. Thus, dispersion coefficients for both thermal dispersion and particle mechanical dispersion were estimated, using pore-scale profiles for velocity and temperature. It has been found that the present analytical expression for the transverse

thermal dispersion based on the pore-scale analysis closely follows the empirical correlation of Calmidi & Mahajan (2000). The longitudinal particle mechanical dispersion works either to suppress or to enhance the effective diffusion depending on the sign of the local phase temperature difference, while the transverse counterpart is insignificant and therefore can be neglected. Moreover, a comparison under equal pumping power revealed that a high level of the heat transfer rate (about 80 times more than the case of base fluid convection without a metal foam) may be achieved by a combination of metal foam and nanofluid.

List of symbols

A	Surface area (m^2)
a_f	Specific surface (m^{-1})
A_{int}	Interfacial area between the fluid and solid (m^2)
c	Specific heat of nanofluid (J kg^{-1} K^{-1})
c_p	Specific heat of nanoparticle (J kg^{-1} K^{-1})
c_s	Specific heat of solid phase (J kg^{-1} K^{-1})
Da	Darcy number
D_B	Brownian diffusion coefficient (m^2 s^{-1})
D_T	Thermophoretic diffusion coefficient (m^2 s^{-1})
d_m	Mean pore diameter (m)
d_p	Nanoparticle diameter (m)
f, F, g, G	Profile functions
Hg	Hagen number
h	Wall heat transfer coefficient (W m^{-2} K^{-1})
h_v	Volumetric heat transfer coefficient (W m^{-3} K^{-1})
H	Channel height (m)
k	Thermal conductivity of nanofluid (W m^{-1} K^{-1})
k_{BO}	Boltzmann constant (J K^{-1})
k_{dis}	Dispersion thermal conductivity (W m^{-1} K^{-1})
k_{stag}	Stagnant thermal conductivity (W m^{-1} K^{-1})
K	Permeability (m^2)
Nu_v	Interstitial Nusselt number
Le	Lewis number
n_j	Unit vector pointing outwards from fluid side to solid side
n_{BT}	Microscopic Brownian and thermophoretic diffusivity ratio
N_{BT}	Macroscopic Brownian and thermophoretic diffusivity ratio
$Nu_{H,R}$	Nusselt number
Nu_v	Interstitial Nusselt number
p	Pressure (Pa)
Pe	Péclet number
Pr	Prandtl number of nanofluid
P.P.	Dimensionless pumping power
q_0	Wall heat flux (W m^{-2})
r	Radial coordinate (m)

R	Tube radius (m)
t	Time (s)
T	Absolute temperature (K)
u_i	Velocity vector (m s^{-1})
V	Representative elementary volume (m^3)
x_i	Cartesian coordinates (m)
x, y, z	Cartesian coordinates (m)
γ	Parameter associated with temperature ratio
ε	Porosity
ε^*	Effective porosity
ς_k	Transverse thermal dispersion coefficient
η $(\zeta = 1 - \eta)$	Dimensionless radial coordinate
μ	Viscosity (Pa s)
ν	Kinematic viscosity of nanofluid (m^2 s^{-1})
ρ	Density of nanofluid (kg m^{-2})
ϕ	Nanoparticle volume fraction

Special symbols

$\tilde{\varphi}$	Deviation from intrinsic average
$\bar{\varphi}$	Average over the cross-section
φ^*	Dimensionless variable
$\langle\varphi\rangle$	Darcian average
$\langle\varphi\rangle^{f,s}$	Intrinsic average

Subscripts and superscripts

B	Bulk mean
bf	Base fluid
dis	Dispersion
f	Fluid phase
p	Nanoparticle
s	Solid phase
w	Wall

REFERENCES

BIANCO, V., CHIACCHIO, F., MANCA, O. & NARDINI, S. 2009 Numerical investigation of nanofluids forced convection in circular tubes. *Appl. Therm. Engng* **29** (17–18), 3632–3642.

BUONGIORNO, J. 2006 Convective transport in nanofluids. *Trans. ASME: J. Heat Transfer* **128**, 240–250.

CALMIDI, V. V. & MAHAJAN, R. L. 1999 The effective thermal conductivity of high porosity fibrous metal foams. *Trans. ASME: J. Heat Transfer* **121**, 466–471.

CALMIDI, V. V. & MAHAJAN, R. L. 2000 Forced convection in high porosity metal foams. *Trans. ASME: J. Heat Transfer* **122**, 557–565.

CHENG, P. 1978 Heat transfer in geothermal systems. *Adv. Heat Transfer* **14**, 1–105.

CHIEN, R. & CHUANG, J. 2007 Experimental microchannel heat sink performance studies using nanofluids. *Intl J. Therm. Sci.* **46**, 57–66.

DUKHAN, N. 2013 *Metal Foams: Fundamentals and Applications*. DEStech Publications.

FRIED, J. J. & COMBARNOUS, M. A. 1971 Dispersion in porous media. *Adv. Hydrosci.* **7**, 169–282.

GELHAR, L. W. & CARL, L. A. 1983 Three-dimensional stochastic analysis of macrodispersion in aquifers. *Water Resour. Res.* **19** (1), 161–180.

HERIS, S. Z., ESFAHANY, M. N. & ETEMAD, S. G. 2007 Experimental investigation of convective heat transfer of Al_2O_3/water nanofluid in a circular tube. *Intl J. Heat Fluid Flow* **28**, 203–210.

KUWAHARA, F., YANG, C., ANDO, K. & NAKAYAMA, A. 2011 Exact solutions for a thermal nonequilibrium model of fluid saturated porous media based on an effective porosity. *Trans. ASME: J. Heat Transfer* **133**, 112602.

LAUNDER, B. E. & SPALDING, D. B. 1974 The numerical computation of turbulent flow. *Comput. Meth. Appl. Mech. Engng* **3**, 269–289.

LEE, S. & CHOI, S. U. S. 1996 Application of metallic nanoparticle suspensions in advanced cooling systems. *International Mechanical Engineering Congress and Exhibition, 17–22 November 1966, Atlanta, USA*. pp. 1–12.

LEE, S., CHOI, S. U. S., LI, S. & EASTMAN, J. A. 1999 Measuring thermal conductivity of fluids containing oxide nanoparticles. *Trans. ASME: J. Heat Transfer* **121**, 280–289.

LI, W. & NAKAYAMA, A. 2015 Temperature dependency of thermophysical properties in convective heat transfer enhancement in nanofluids. *J. Thermophys. Heat Transfer* **29** (2), (in press).

LIANG, C. Y. & YANG, W. J. 1975 Modified single blow technique for performance evaluation on heat transfer surfaces. *Trans. ASME: J. Heat Transfer* **97**, 16–21.

MAIGA, S. B., PALM, S. J., NGUYEN, C. T., ROY, G. & GALANIS, N. 2005 Heat transfer enhancement by using nanofluids in forced convection flows. *Intl J. Heat Fluid Flow* **26**, 530–546.

NAKAYAMA, A. 1995 *PC-Aided Numerical Heat Transfer and Convective Flow*, pp. 49–50, 103–115. CRC Press.

NAKAYAMA, A., ANDO, K., YANG, C., SANO, Y., KUWAHARA, F. & LIU, J. 2009 A study on interstitial heat transfer in consolidated and unconsolidated porous media. *Heat Mass Transfer* **45** (11), 1365–1372.

NAKAYAMA, A., KUWAHARA, F. & HAYASHI, T. 2004 Numerical modelling for three-dimensional heat and fluid flow through a bank of cylinders in yaw. *J. Fluid Mech.* **498**, 139–159.

NAKAYAMA, A., KUWAHARA, F. & KODAMA, Y. 2006 An equation for thermal dispersion flux transport and its mathematical modelling for heat and fluid flow in a porous medium. *J. Fluid Mech.* **563**, 81–96.

OHSAWA, S. 2015 Three-dimensional simulation of heat and fluid flow in a nanofluid saturated metal foam. Master thesis, Graduate School of Engineering, Shizuoka University, Japan.

PAK, B. C. & CHO, Y. 1998 Hydrodynamic and heat transfer study of dispersed fluids with submicron metallic oxide particles. *Exp. Heat Transfer* **11**, 151–170.

QUINTARD, M. & WHITAKER, S. 1993 One and two equation models for transient diffusion processes in two-phase systems. *Adv. Heat Transfer* **23**, 369–465.

QUINTARD, M. & WHITAKER, S. 1995 Local thermal equilibrium for transient heat conduction: theory and comparison with numerical experiments. *Intl J. Heat Mass Transfer* **38**, 2779–2796.

SAKAI, F., LI, W. & NAKAYAMA, A. 2014 A rigorous derivation and its applications of volume averaged transport equations for heat transfer in nanofluid saturated metal foam, *Proceedings of the International Heat Transfer Conference, 10–15 August 2014, Kyoto, Japan.*

TAYLOR, G. I. 1953 Dispersion of soluble matter in solvent flowing slowly through a tube. *Proc. R. Soc. Lond.* A **219**, 186–203.

TAYLOR, G. I. 1954 The dispersion of matter in turbulent flow through a pipe. *Proc. R. Soc. Lond.* A **223**, 446–468.

WANG, J. & KITANIDIS, P. K. 1999 Analysis of macrodispersion through volume averaging: comparison with stochastic theory. *Stoch. Environ. Res. Risk Assess.* **13**, 66–84.

XUAN, Y. & ROETZEL, W. 2000 Conceptions for heat transfer correlations of nanofluids. *Intl J. Heat Mass Transfer* **43**, 3701–3707.

YANG, C., ANDO, K. & NAKAYAMA, A. 2011 A local thermal non-equilibrium analysis of fully developed forced convective flow in a tube filled with a porous medium. *Trans. Porous Med.* **89**, 237–249.

YANG, C., LI, W. & NAKAYAMA, A. 2013*a* Convective heat transfer of nanofluids in a concentric annulus. *Intl J. Therm. Sci.* **71**, 249–257.

YANG, C., LI, W., SANO, Y., MOCHIZUKI, M. & NAKAYAMA, A. 2013*b* On the anomalous convective heat transfer enhancement in nanofluids: a theoretical answer to the nanofluids controversy. *Trans. ASME: J. Heat Transfer* **135**, 054504.

YANG, C., LIU, W. & NAKAYAMA, A. 2009 Forced convective heat transfer enhancement in a tube with its core partially filled with a porous medium. *Open Transp. Phenom. J.* **1**, 1–6.

YANG, C. & NAKAYAMA, A. 2010 A synthesis of tortuosity and dispersion in effective thermal conductivity of porous media. *Intl J. Heat Mass Transfer* **53**, 3222–3230.

ZHUKAUSKAS, A. 1987 Heat transfer from tubes in crossflow. *Adv. Heat Transfer* **18**, 87–159.